Universität des Saarlandes

Fachrichtung 6.1 – Mathematik

Preprint Nr. 281

Perspective Shape from Shading: Ambiguity Analysis and Numerical Approximations

Michael Breuß, Emiliano Cristiani, Jean-Denis Durou,
Maurizio Falcone and Oliver Vogel

Saarbrücken 2010

Fachrichtung 6.1 – Mathematik
Universität des Saarlandes

Preprint No. 281
submitted: November 8, 2010

Perspective Shape from Shading: Ambiguity Analysis and Numerical Approximations

Michael Breuß
Saarland University
Faculty of Mathematics and Computer Science
Building E1.1, 66041 Saarbrücken, Germany
breuss@mia.uni-saarland.de

Emiliano Cristiani
Dipartimento di Matematica
SAPIENZA - Università di Roma
P.le Aldo Moro 2, 00185 Rome, Italy
emiliano.cristiani@gmail.com

Jean-Denis Durou
Institut de Recherche en Informatique de Toulouse
Université Paul Sabatier
118 route de Narbonne, 31062 Toulouse Cédex 9, France
and
Centre de Mathématiques et de Leurs Applications
École Normale Supérieure de Cachan
61 avenue du président Wilson, 94235 Cachan Cédex, France
durou@cmla.ens-cachan.fr

Maurizio Falcone
Dipartimento di Matematica
SAPIENZA - Università di Roma
P.le Aldo Moro 2, 00185 Rome, Italy
falcone@mat.uniroma1.it

Oliver Vogel
Saarland University
Faculty of Mathematics and Computer Science
Building E1.1, 66041 Saarbrücken, Germany
vogel@mia.uni-saarland.de

Edited by
FR 6.1 – Mathematik
Universität des Saarlandes
Postfach 15 11 50
66041 Saarbrücken
Germany

Fax: + 49 681 302 4443
e-Mail: preprint@math.uni-sb.de
WWW: http://www.math.uni-sb.de/

Abstract

In this paper we study a modern, perspective model for shape from shading and its numerical approximation. We show that a new form of the classic concave/convex ambiguity is still present, although the model has been shown to be well-posed under particular assumptions. This analytical result is confirmed by various numerical tests. Moreover, we present convergence results for two iterative approximation schemes recently introduced in the literature. The first one is based on a finite difference discretization, whereas the second one is based on a semi-Lagrangian discretization. The convergence results are obtained in the general framework of viscosity solutions of the underlying partial differential equation. We also show that it is possible to obtain even in complex scenes results of reasonable quality. To this end we solve the constituting equation on a previously-segmented input image, where we use state constraints boundary conditions at the segment borders.

1 Introduction

The shape-from-shading (SFS) problem amounts to the reconstruction of the 3-D structure of objects at hand of a single given 2-D grey value image of them. For this task, the SFS process relies on information on the illumination and the light reflectance in the scene. It has been introduced by Horn [15], and it is a classic inverse problem in computer vision with many potential applications, see e.g. [12, 16, 17, 34] and the references therein for an overview.

In this paper we deal with a modern SFS model proposed by Prados and Faugeras [24, 27]. This SFS model has gained some attention in the recent literature. It combines desirable theoretical properties with a reasonable quality of results compared to other approaches in SFS. One of its good theoretical properties is the well-posedness given under some assumptions. However, the question arises whether the notorious concave/convex ambiguity [15] has entirely been vanquished by using the SFS model of Prados and Faugeras. For the case that the answer is negative, it would be of interest if there is a way to avoid ambiguities. Concerning the numerical realization of the model, a number of iterative solvers has been proposed. However, while the two most efficient schemes have been identified [4], their mathematical validation is lacking.

In this paper we address these open issues. By a thorough investigation, we show that a concave/convex ambiguity still arises and appears in practical computations. We propose a way how such ambiguities can be avoided by making use of a segmentation step combined with suitable boundary conditions at the segment borders. In this way, also shapes in relatively complex scenes can be reconstructed. Moreover, we prove that the two currently best iterative solvers converge to the viscosity solution of the considered equation.

Models and ambiguities Perspective SFS models are distinguished by the assumption that the camera performs a perspective projection of the 3-D world to the given 2-D image. Recently, a number of perspective SFS models have been considered [8, 24, 30],

with promising applications to face reconstruction [24], reconstruction of organs [30, 31], and digitization of documents [8, 9].
Within the class of perspective SFS models, the one of Okatani and Deguchi [20] is distinguished by the lighting model. This consists of a point light source located at the optical center combined with a light attenuation term. Okatani and Deguchi proposed a method to resolve their model which is an extension of the level set method designed by Kimmel et al. [18] for solving the classic SFS problem. They claim that their method could be derived from a PDE of the form $H(x, y, r, r_x, r_y) = 0$, where r is the distance to the point light source, but do not explicitly state it. Prados and Faugeras [27] stated the first PDE derived from this model that we call here the *PSFS model* ('P' for 'perspective'). A number of papers by Prados and his coauthors have dealt with its theoretical basis, cf. [22, 23, 26, 27]. Especially, the PSFS model has been shown to be well-posed under mild assumptions.
The well-posedness of SFS models has been a point of continuous interest in computer vision research. This already begins with Horn [15] who mentions the concave/convex ambiguity in his classic orthographic SFS model; see [6, 17] for extensive discussion. Two main features for proofs of existence and uniqueness of the solution are the singular points and the edges [2, 5, 6, 13, 21], since the surface normal in such points can be computed without ambiguity.
It turns out that the classic concave/convex ambiguity is not the only source of non-uniqueness. Starting from a paper by Rouy and Tourin [29], a modern tool to understand the hyperbolic partial differential equations (PDEs) that arise in SFS is the notion of viscosity solutions. For the classic SFS model investigated in [29], one can see that this notion allows several weak solutions in the viscosity sense. This lack of uniqueness is a fundamental property of the underlying class of PDEs. In order to achieve uniqueness in this setting, one may add information such as the height at each singular point [19], or one may characterize the so-called maximal solution [7, 14].

Numerical methods for PSFS A number of recent papers have considered the numerical realization of the PSFS model. The original scheme of Prados et al., see especially [22], relies on the optimal control formulation of the PSFS model. It solves the underlying Hamilton-Jacobi-Bellman equation using a top-down dynamic programming approach. However, the method is difficult to implement as it relies on the analytical solution of an incorporated optimization problem involving many distinct cases. In [11] a semi-Lagrangian method (CFS) has been proposed. This method also relies on the Hamilton-Jacobi-Bellman equation but it is much easier to code. An alternative approach has been explored in [33] where the Hamilton-Jacobi equation corresponding to the PSFS model has been discretized with finite differences (VBW).
All the mentioned schemes as well as their algorithmic extensions have been studied experimentally in [4]. The latter two schemes, i.e. CFS and VBW, have been identified as the most efficient techniques.

Our contribution The novelties of this paper can be summarized as follows:

(i) We explain in detail why the PSFS model cannot be considered completely well-posed as concluded in [27, 28]. To this end, we show analytically that a new class of *generalized concave/convex ambiguity* arises, and we present numerical computations proving the practical importance of this new type of ambiguities.

(ii) We prove convergence to the viscosity solution of both the CFS [11] and the VBW [33] scheme.

For validating the convergence of the VBW method, we show how to make use of previous results of Barles and Souganidis [1]. Concerning the proof of convergence for the CFS scheme, we do not rely on that classic approach. Our proof relies on the idea that the CFS iterates are monotone decreasing (in the sense of pointwise comparison) as well as bounded from below, which implies convergence. A similar strategy has been developed in [3] in the context of hyperbolic conservation laws.

(iii) Relying on the results from *(i)* and *(ii)*, we explore an algorithmic way to overcome ambiguities via a pre-segmentation of the input image. This allows to approximate the smooth parts of the PSFS solution with correct initial conditions for iterative methods. At segment borders that usually coincide in computations with points of non-continuity or non-differentiability, state constraints boundary conditions are employed. We validate experimentally using synthetic and real-world data that this set-up gives reasonable results.

Our work shows that a complete understanding combining the theoretical analysis of the PDE and the numerical analysis of solution schemes is useful for dealing with complex computer vision problems such as PSFS.

Paper organization The paper is organized as follows. In Section 2, we briefly review the model and the related equations. The ambiguity problem is discussed in detail in Section 3. The numerical methods and their convergence are considered in Section 4. Section 5 is devoted to numerical experiments. The paper is finished by a conclusion. Some technical issues are described in appendices.

2 The PSFS model and related equations

In this section, we recall, for the reader's convenience, the model for PSFS with point light source located at the optical center and light attenuation term. We also recall the first related PDE associated to the model, derived in [28].

2.1 The PSFS model with light attenuation

Let (x, y) be a point in the image domain Ω, where Ω is an open bounded subset of $\mathbb{R}^2$. Furthermore, let

- $I = I(x, y) > 0$ be the normalised brightness function. We have $I = \frac{E(x,y)}{\sigma}$, where E is the greylevel of the given image and σ is the product of the surface albedo (which tells us to which extent the surface reflects light) and the light source intensity;
- f be the focal length, i.e. the distance between the optical center C of the camera and the two-dimensional plane to which the scene of interest is mapped (see Fig. 1).

Let M be a generic point on the surface Σ. We choose as unknown of the problem the function $u : \Omega \to \mathbb{R}$ such that

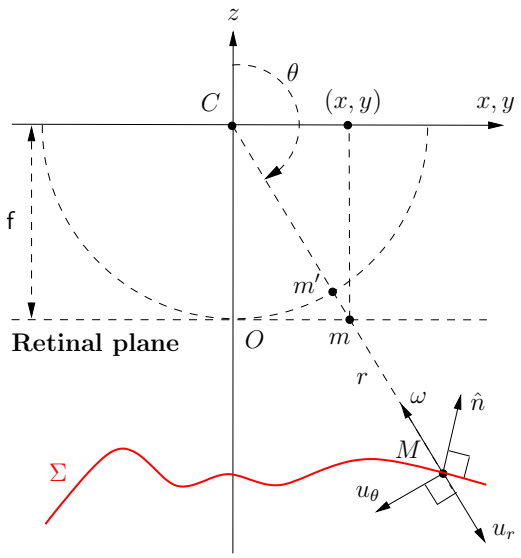

Figure 1: Notations for the perspective SFS model with point light source at optical center.

$$M = M(x, y) = u(x, y)\, m', \tag{1}$$

where

$$m' = \frac{\mathsf{f}}{\sqrt{x^2 + y^2 + \mathsf{f}^2}}\, m \quad \text{and} \quad m = (x, y, -\mathsf{f})^\top. \tag{2}$$

Another definition of the unknown u is given by the relation $M(x, y) = u(x, y)\, m$, which differs from (1) and leads to a slightly different PDE, as shown in [28].
Note that, according to these notations, $u > 0$ holds as the depicted scene is in front of the camera. We denote by $r(x, y)$ the distance between the point light source and the point $M(x, y)$ on the surface. It holds $u(x, y) = r(x, y)/\mathsf{f}$, since the light source location coincides with the optical center.
The model associated to the PSFS problem is obtained by the *image irradiance equation*:

$$R(\widehat{n}(x, y)) = I(x, y), \tag{3}$$

making explicit the unit normal $\widehat{n}$ to the surface and the reflectance function R which gives the value of the light reflection on the surface as a function of its normal.
We denote by $\omega(x,y)$ the unit vector representing the light source direction at the point $M(x,y)$ (note that in the classic SFS model this vector is constant):

$$\omega(x,y) = \frac{(-x,-y,\mathsf{f})^\top}{\sqrt{x^2+y^2+\mathsf{f}^2}}. \tag{4}$$

Adding the assumptions of a *light attenuation term* and of a *Lambertian surface*, the function R is defined as

$$R(\widehat{n}(x,y)) = \frac{\omega(x,y)\cdot\widehat{n}(x,y)}{r(x,y)^2}, \tag{5}$$

with an attenuation factor which is equal to the inverse of the squared distance from the source. Expression (5) would still hold for any location of the point light source, but the same would not be true for the equality $u(x,y) = r(x,y)/\mathsf{f}$ nor for (4). The case where the light source coincides with the optical center is not only that which gives the simplest model: it more or less corresponds to endoscopic images [20] and to photographs taken at short distance with the camera flash [28]. Another considerable advantage of the PSFS model using a point light source at the optical center is that there is no shadow in the image.
Finally, by (3) and (5) we obtain the PSFS equation

$$\frac{\omega(x,y)\cdot\widehat{n}(x,y)}{r(x,y)^2} = I(x,y). \tag{6}$$

2.2 The corresponding Hamilton-Jacobi equation

In order to write down the corresponding PDE, it is useful to introduce the new unknown $v = \ln(u)$ (we recall that $u > 0$). Equation (6) can be written [27, 28] as a static Hamilton-Jacobi equation (see [28], and Appendix A for details):

$$H(x,y,v,\nabla v) := \frac{I(x,y)}{Q(x,y)}\,\mathsf{f}^2\,W(x,y,\nabla v) - e^{-2v(x,y)} = 0\,, \quad (x,y)\in\Omega \tag{7}$$

where

$$Q(x,y) := \frac{\mathsf{f}}{\sqrt{x^2+y^2+\mathsf{f}^2}} \tag{8}$$

(which is equal to $|\cos\theta|$, cf. Fig. 1) and

$$W(x,y,\nabla v) := \sqrt{\mathsf{f}^2\|\nabla v\|^2 + (\nabla v\cdot(x,y))^2 + Q(x,y)^2}, \tag{9}$$

($\|\cdot\|$ denotes the Euclidean vector norm). Note that $W(x,y,\nabla v)$ is convex with respect to $\nabla v\in\mathbb{R}^2$, and then the Hamiltonian $H(x,y,v,\cdot)$ is convex.
The existence and uniqueness of the viscosity solution of equation (7) is proven in [28]. In the same paper some possible choices for the boundary conditions are discussed.

Equation (7) also admits a "control formulation" which can be helpful. In [28] it is shown that v is the solution of the following Hamilton-Jacobi-Bellman-like equation

$$-e^{-2v(x,y)} + \sup_{a \in \overline{B(0,1)}} \{-b(x,y,a) \cdot \nabla v(x,y) - \ell(x,y,a)\} = 0 \tag{10}$$

where $\overline{B(0,1)}$ denotes the closed unit ball in $\mathbb{R}^2$ and the other terms in (10) are defined as follows:

$$b(x,y,a) := -JG^T DGa\,, \quad \ell(x,y,a) := -I(x,y)\,\mathsf{f}^2\,\sqrt{1-\|a\|^2}\,, \tag{11}$$

$$J(x,y) := \frac{I(x,y)}{Q(x,y)}\mathsf{f}^2 = I(x,y)\mathsf{f}\sqrt{\mathsf{f}^2+x^2+y^2} \tag{12}$$

where G, D are the 2×2 matrices

$$G(x,y) := \begin{cases} \frac{1}{\sqrt{x^2+y^2}} \begin{pmatrix} y & -x \\ x & y \end{pmatrix} & \text{if } (x,y) \neq (0,0) \\ \begin{pmatrix} 1 & 0 \\ 0 & 1 \end{pmatrix} & \text{if } (x,y) = (0,0) \end{cases},$$

$$D(x,y) := \begin{pmatrix} \mathsf{f} & 0 \\ 0 & \sqrt{\mathsf{f}^2+x^2+y^2} \end{pmatrix}.$$

3 The generalized concave/convex ambiguity

In this section, we show that in the model presented above an analogue of the classic concave/convex ambiguity still exists. We also show in detail in which case it is numerically possible to reconstruct the expected surface and in which case a different surface is computed. After rewriting the PSFS equation in spherical coordinates, we will restrict ourself to the one-dimensional case. This is done to make the theoretical and numerical analysis simpler, and it is sufficient to show the presence of an ambiguity in the model. Indeed, if an ambiguity appears in the one-dimensional case, *a fortiori* it appears in the two-dimensional case.

3.1 The ambiguity in the model

In order to prove the existence of at least two different surfaces which are associated to the same brightness function I and the same Dirichlet boundary conditions, it is convenient to reformulate the problem in standard spherical coordinates (r,θ,ϕ): the parameters of an image point $m(\theta,\phi)$ are now the angles θ and ϕ, which are respectively the colatitude and the longitude of the conjugated object point $M(\theta,\phi)$, with respect to the camera coordinate system $(Cxyz)$. Let us notice that only the object points $M(\theta,\phi)$ such that $\theta \in [\pi/2,\pi]$

are visible (see Figure 1), whereas $\phi \in [0, 2\pi[$. Given a brightness function $I(\theta, \phi)$, we are looking for a surface Σ in the form $r = r(\theta, \phi)$ such that:

$$\frac{\omega(\theta, \phi) \cdot \widehat{n}(\theta, \phi)}{r(\theta, \phi)^2} = I(\theta, \phi). \tag{13}$$

A generic point M has coordinates:

$$M(\theta, \phi) = \begin{pmatrix} r(\theta, \phi) \sin\theta \cos\phi \\ r(\theta, \phi) \sin\theta \sin\phi \\ r(\theta, \phi) \cos\theta \end{pmatrix}_{(Cxyz)} \tag{14}$$

with respect to the coordinate system $(Cxyz)$. We now introduce the local orthonormal basis $\mathcal{S} = (u_r, u_\theta, u_\phi)$ of $\mathbb{R}^3$ defined by:

$$u_r := \frac{M(\theta, \phi)}{r(\theta, \phi)}, \qquad u_\theta := \frac{\partial_\theta u_r}{\|\partial_\theta u_r\|} \qquad \text{and} \qquad u_\phi := \frac{\partial_\phi u_r}{\|\partial_\phi u_r\|}, \tag{15}$$

which depends on the point M (see Fig. 1). The expression of $\widehat{n}$ in this new basis is (see Appendix B for details):

$$\widehat{n}(\theta, \phi) = \frac{1}{((r^2 + {r_\theta}^2)\sin^2\theta + {r_\phi}^2)^{1/2}} \begin{pmatrix} -r\sin\theta \\ r_\theta \sin\theta \\ r_\phi \end{pmatrix}_{\mathcal{S}}, \tag{16}$$

where the dependences of r, r_θ and r_ϕ on (θ, ϕ) are omitted. Using the expression (16) of $\widehat{n}$, and knowing that ω coincides with $-u_r$, since the point light source is located at the optical center, Equation (13) can be rewritten as:

$$r^2 \left(r^2 + {r_\theta}^2 + \frac{{r_\phi}^2}{\sin^2\theta} \right) = \frac{1}{I^2}. \tag{17}$$

We now return to our purpose. We choose as reference surface $\overline{\Sigma}$ the hemisphere $r(\theta, \phi) \equiv 1$, where $(\theta, \phi) \in [\pi/2, \pi] \times [0, 2\pi[$, which is associated to the brightness function $I_{\overline{\Sigma}}(\theta, \phi) \equiv 1$ (see Figure 2-a). Then, we look for other surfaces which are not isometric to $\overline{\Sigma}$ but give the same brightness function. For the sake of simplicity, let us limit our search to the surfaces which are circularly-symmetric around the optical axis Cz i.e., to the functions r of the form $r(\theta, \phi) = r(\theta)$. Equation (17) is thus simplified to the following ordinary differential equation:

$$r^2(r^2 + {r_\theta}^2) = \frac{1}{{I_{\overline{\Sigma}}}^2} = 1, \tag{18}$$

which can be rewritten, since Equation (18) imposes that $r \leq 1$:

$$\frac{r\, dr}{\sqrt{1 - r^4}} = \pm d\theta. \tag{19}$$

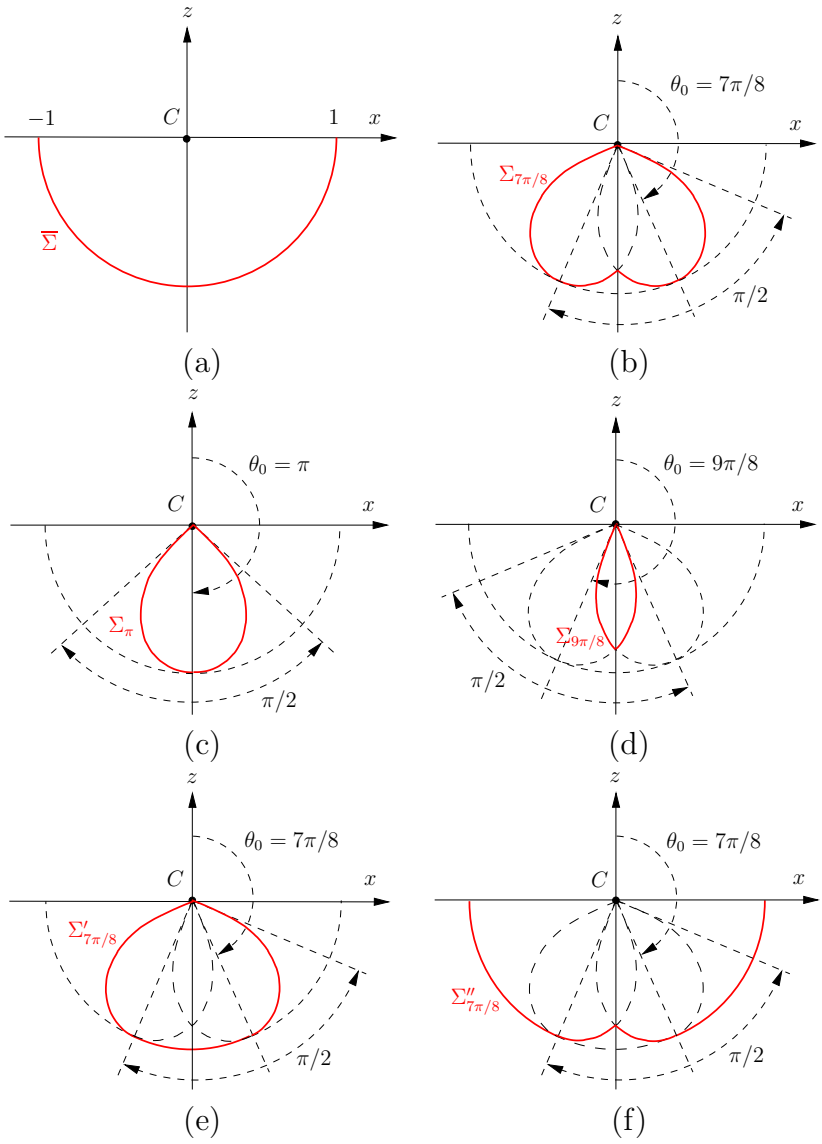

Figure 2: Generalized concave/convex ambiguity. All the surfaces drawn in red solid line, which are circularly-symmetric around the optical axis Cz, have the same image with uniform greylevel $I \equiv 1$ as the hemisphere $\overline{\Sigma}$ shown in (a), according to the perspective shape-from-shading model with point light source at the optical center and light attenuation: (b), (c) and (d) show three surfaces $\Sigma_{7\pi/8}$, Σ_π and $\Sigma_{9\pi/8}$ among the continuous family $\{\Sigma_{\theta_0}\}_{\theta_0 \in [3\pi/4, 5\pi/4]}$; (e) and (f) show two other surfaces $\Sigma'_{7\pi/8}$ and $\Sigma''_{7\pi/8}$ that can be constructed by joining $\Sigma_{7\pi/8}$ to $\overline{\Sigma}$: $\Sigma'_{7\pi/8}$ is of class C^1, whereas $\Sigma''_{7\pi/8}$ is differentiable everywhere except in its intersection with the optical axis.

Integrating Equation (19), we obtain the following solutions depending on a parameter θ_0,

which is a constant of integration:

$$r_{\theta_0}(\theta) = \sqrt{\cos(2(\theta - \theta_0))}. \tag{20}$$

Let us denote as Σ_{θ_0} the surface of equation $r = r_{\theta_0}(\theta)$. Note that equation (20) imposes that $\theta \in [\theta_0 - \pi/4, \theta_0 + \pi/4]$. We know that $\theta \in [\pi/2, \pi]$ by definition, then each surface Σ_{θ_0} has the same brightness function $I \equiv 1$ as $\overline{\Sigma}$ in a domain $\mathcal{D}_{\theta_0}$ of the image plane which is circularly-symmetric around the optical axis Cz, and contains the points such that $\theta \in \mathcal{I}_{\theta_0} = [\theta_0 - \pi/4, \theta_0 + \pi/4] \cap [\pi/2, \pi]$. If we impose $\mathcal{D}_{\theta_0}$ to be non-empty and to contain the origin $O = (0, 0)$ in the image plane, this clearly implies that the parameter θ_0 in Equation (20) is in the interval $[3\pi/4, 5\pi/4]$. Then, it is easy to see that $\mathcal{I}_{\theta_0} = [\theta_0 - \pi/4, \pi]$ and that $\mathcal{D}_{\theta_0}$ is a disc of center O and of radius $\rho_{\theta_0} = \mathsf{f} \tan(5\pi/4 - \theta_0)$.
Since all the surfaces Σ_{θ_0}, for $\theta_0 \in [3\pi/4, 5\pi/4]$, are circularly-symmetric around the optical axis Cz, we only draw their cuts by the plane Cxz. Three such cuts are represented in Figures 2-b,c,d (note that we have simplified here the three-dimensional setting of spherical coordinates to two dimensions, omitting the angle describing the location of points with respect to the y-axis). Note that among those surfaces, only Σ_π is differentiable everywhere (see Figure 2-c). We thus found two differentiable surfaces $\overline{\Sigma}$ and Σ_π giving the same image in the disc $\mathcal{D}_\pi = (O, \mathsf{f})$ under the PSFS model with point light source at the optical center and light attenuation term. Since this recalls the well-known concave/convex ambiguity of the classic SFS model, we refer to this new ambiguity as the *generalized concave/convex ambiguity*.
It is important to stress that all the surfaces Σ_{θ_0}, for $\theta_0 \in [3\pi/4, 5\pi/4] \backslash \{\pi\}$, have a unique singularity at their intersection with the optical axis. Moreover each surface Σ_{θ_0}, for $\theta_0 \in [3\pi/4, \pi[$, is tangent to the reference surface $\overline{\Sigma}$ in $\theta = \theta_0$, so that other differentiable (but not of class C^2) solutions can be constructed by joining the differentiable part of Σ_{θ_0} to $\overline{\Sigma}$. These new surfaces are called Σ'_{θ_0} (see Figure 2-e). Finally, the non-differentiable part of Σ_{θ_0} can be joined to $\overline{\Sigma}$. These last solutions are called Σ''_{θ_0} (see Figure 2-f). We thus found four families of continuous surfaces associated to the same image than $\overline{\Sigma}$, namely $\{\Sigma_{\theta_0}\}_{\theta_0 \in [3\pi/4, \pi[}$, $\{\Sigma_{\theta_0}\}_{\theta_0 \in]\pi, 5\pi/4]}$, $\{\Sigma'_{\theta_0}\}_{\theta_0 \in [3\pi/4, \pi[}$, and $\{\Sigma''_{\theta_0}\}_{\theta_0 \in [3\pi/4, \pi[}$, which are illustrated, respectively, in Figures 2-b,d,e,f. The surfaces Σ'_{θ_0} are differentiable everywhere (but are not of class C^2) and they are the only C^1 solutions. In the next subsection, we will see that $\overline{\Sigma}$, which constitutes a common super-solution of all these solutions, is the initial surface used in the algorithm of Prados et al. [28].
Let us also mention that, among the different solutions of our problem, a certain number share a part of the boundary conditions. This is the case, for instance, of Σ_{θ_0}, Σ'_{θ_0} and Σ''_{θ_0}, for $\theta_0 \in [3\pi/4, \pi[$, on the circle where these three surfaces are tangent to $\overline{\Sigma}$ (note that either the Dirichlet and the Neumann conditions are identical there).
Let us finally note that the greylevel remains unchanged by rotation of all these surfaces around the optical center C, since it is uniformly equal to 1. This leads us to other solutions, which are not circularly-symmetric around the optical axis any more. We will see in the next subsection that all of these solutions can be computed by solving the PSFS equation (7) imposing appropriate boundary conditions.

3.2 Viscosity and weak solutions

In this subsection we investigate when the generalized concave/convex ambiguity arises solving the PSFS equation (7). The uniqueness of the viscosity solution of equation (7) was proven in [28] (see also [26]). Nevertheless, the uniqueness of the viscosity solution does not solve the problem of the model ambiguity, because we could be interested in the reconstruction of a surface not described by the viscosity solution, rather by another weak solution. This is a well-known issue in orthographic SFS with light beam parallel to the optical axis: let us consider the simple case of a one-dimensional greylevel image with constant brightness function $I(x) \equiv \sqrt{2}/2$, and let us solve the SFS problem by means of the eikonal equation

$$|z'(x)| = \sqrt{\frac{1}{I^2(x)} - 1}\,, \qquad x \in [-1, 1] \tag{21}$$

imposing exact Dirichlet boundary conditions $z = 0$ at $x = -1$ and $x = 1$. Here $z(x)$ denotes the height of the surface. The unique viscosity solution is drawn in Fig. 3-a, while other possible (weak) solutions are drawn in Fig. 3-b. Our goal is to show that the PSFS

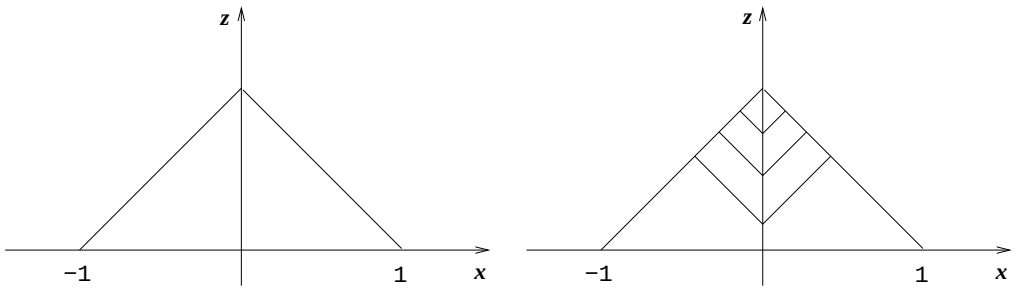

Figure 3: (a) Viscosity solution and (b) some weak solutions of the eikonal equation (21).

equation (7) has essentially the same features of the eikonal equation (21), thus showing the same kind of ambiguity. The starting point is the following Proposition.

Proposition 3.1 *The viscosity solution $u = e^v$ of the* PSFS *equation (7) is increasing along characteristic curves.*

Proof Let us define

$$\overline{u}(x, y) := (I(x, y)\mathsf{f}^2)^{-\frac{1}{2}}\,, \tag{22}$$

corresponding to

$$\overline{v}(x, y) := \ln(\overline{u}(x, y)) = -\frac{1}{2}\ln(I(x, y)\mathsf{f}^2). \tag{23}$$

Let us prove that the inequality

$$\overline{u}(x, y) \geq u(x, y) \qquad \forall (x, y) \in \Omega \tag{24}$$

(and similarly $\overline{v} \geq v$) holds. Equation (24) easily follows from equation (6) and from the definition $u = r/\mathsf{f}$, since $\overline{u}$ is the solution of the equation where $\omega \cdot \widehat{n} = 1$ and it is larger than the solution u where $\omega \cdot \widehat{n} < 1$. In [28] it is also proven that $\overline{v}$ is a super-solution of the equation (7). Note that, in the example of Fig. 3.1, the super-solution $\bar{u}$ corresponds to the hemisphere shown in Fig. 3.1-a.
Let us consider a point (x, y) where v is differentiable (we recall that v is differentiable everywhere in Ω except for a zero-measure subset) and assume that there exists a control $a^* \in \overline{B(0,1)}$ in which the maximum in Equation (10) is attained. Then Equation (10) can be rewritten as

$$-e^{-2v(x,y)} + (-b(x, y, a^*) \cdot \nabla v(x, y) - \ell(x, y, a^*)) = 0.$$

We have

$$\begin{aligned}
&\frac{\partial v(x,y)}{\partial(-b(x,y,a^*))} = -b(x, y, a^*) \cdot \nabla v(x, y) = \\
&\ell(x, y, a^*) + e^{-2v(x,y)} = -I(x, y)\, \mathsf{f}^2 \sqrt{1 - \|a^*\|^2} + e^{-2v(x,y)} \geq \\
&-I(x, y)\, \mathsf{f}^2 \sqrt{1 - \|a^*\|^2} + e^{-2\overline{v}(x,y)} = I(x, y)\mathsf{f}^2(1 - \sqrt{1 - \|a^*\|^2}) \geq 0\ ,
\end{aligned}$$

which proves our assertion. ♣

As a consequence of the Proposition 3.1, every time the surface we want to reconstruct is described by a function u which is not increasing along characteristics, *it cannot be reconstructed as the viscosity solution of the* PSFS *model*. This is exactly what happens in SFS, see Fig. 3-b. Information spreads from the boundaries to the center of the domain, and the solution can only increase along the way. Then, all the solutions different from the viscosity solution cannot be achieved. To overcome this problem (in SFS as well as PSFS), we can impose the exact solution in every point of local minimum for the solution. Doing this, the correct solution is computed, but we face the new problem of how to recover the values of these new Dirichlet boundary conditions. In this respect, the PSFS model is preferable to the SFS model, since the light attenuation term $1/r^2$ allows to get rid of these additional unknowns. Let us explain this point in detail.

According to Eq. (17), if the surface is differentiable, a local minimum point for u corresponds to a point where $I = 1/r^2$. The latter equation is easily solved with respect to r, and then u is found [32]. This means that the light attenuation term allows to compute the correct solution at the points where we need to impose boundary conditions. It turns out from Eq. (6) that these points are also those where $\omega \cdot \widehat{n} = 1$, which characterizes the so-called *singular points* of the classic SFS model [15].
As we will see in Section 4, the numerical resolution of the PSFS equation needs to set up an iterative procedure, and then an initial guess for u has to be given in order to start the algorithm. Let us denote that initial guess by $u^{(0)}$. If we choose $u^{(0)}$ as

$$u^{(0)} := \overline{u} \tag{25}$$

the algorithm starts from a function which is actually the *correct* solution of the equation (6) at all points where $\omega \cdot \widehat{n} = 1$, and it is *larger* than the correct solution elsewhere. Since the information propagates from the smallest to the largest values, the values larger than the correct ones do not influence the correct ones. Then the values at the local minimum points remain fixed, playing the role of correct Dirichlet boundary conditions, while the other values decreases, converging in the limit to the solution. Note that the initial guess (25) corresponds to the initial guess for v suggested in [28], namely

$$v^{(0)} := \overline{v}. \tag{26}$$

We can conclude that when the surface is differentiable, the PSFS model is well-posed, provided a suitable initial guess for the iterative algorithm is given. Moreover, the correct initial guess can be computed directly from the greylevel image.

If the surface is not differentiable, the method described above cannot be applied. In particular, the method fails whenever one of the following conditions holds true: 1) a point of non-differentiability for the surface is a minimum point, 2) local minimum points coincide with the boundaries, and state constraints boundary conditions are used. In these cases, the initial guess (25) is not able to impose the right values automatically and an ambiguity arises. In order to explain and summarize the role of the initial guess, the minimum points and the boundary conditions, it is useful to consider the four surfaces shown in Fig. 4. Characteristic curves are depicted below the surfaces (although they lie on Ω). The surface in (a) is differentiable, and can be recovered without any additional information. The minimum points for u are automatically detected (black dots on the surface). Characteristics start from these points and the solution increases along them. State constraints boundary conditions are suitable since no information comes from the boundaries. The surface in (b) is not differentiable, but the point of non-differentiability does not coincide with a minimum point for u. Characteristics move away from the minimum points (automatically detected as before), and they meet each other in the point of non-differentiability. The surface in (c) is differentiable, but it cannot be correctly reconstructed unless suitable Dirichlet boundary conditions are given at the boundary of the domain. Indeed, characteristics start from the automatically-detected minimum point, then the solution u is correctly computed from that point until it increases. Near the right-hand boundary, the viscosity solution corresponds to *another surface with the same brightness function*. The surface in (d) is not differentiable, and the point of non-differentiability coincides with a minimum point. Then, one minimum point is not detected and the ambiguity arises in a large part of the domain. Here state constraints are suitable and the surface is correctly reconstructed near the boundaries. To obtain the correct surface, the value of u at the non-differentiable point should be given.

Some numerical approximations for ambiguous cases In order to have a numerical confirmation of the theoretical results presented above, we solved the PSFS equation using the scheme presented in [33], which is proved to be convergent in Section 4. First, we

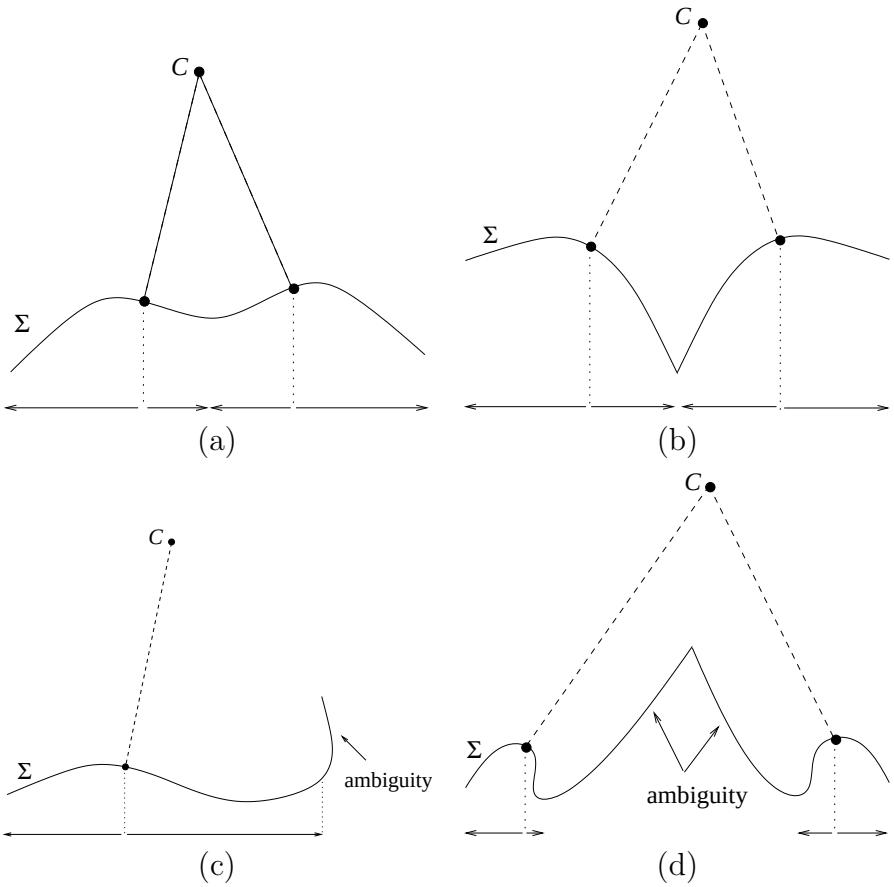

Figure 4: Four surfaces with different properties. Characteristic curves are depicted below the surfaces. (a) differentiable surface, correctly reconstructed imposing state constraints boundary conditions, starting from the two singular points automatically detected (black dots). (b) non differentiable surface, correctly reconstructed as before. (c) differentiable surface with ambiguity if state constraints boundary condition are imposed. The ambiguity is limited in the region where u should increase starting from the source points (black dot). (d) non differentiable surface with ambiguity. The non-differentiable point is not automatically detected.

recovered some of the surfaces described in Fig. 2, choosing a constant brightness function I and then varying the boundary conditions (state constraints or Dirichlet) or imposing specific values in some internal points (see Fig. 5 and its caption). Then, we tried to solve the PSFS problem for two surfaces similar to the surfaces illustrated in Fig. 4-c,d, where an ambiguity is expected. The first surface corresponds to $u(x) = \sin(5x) + 5$, $x \in [-2, 0.8]$. The second surface corresponds to $u(x) = 10|x| + 3$, $x \in [-2, 2]$. For each test we show the initial and the reconstructed surface Σ, together with the functions u and the corresponding brightness functions I. The focal length is set to $\mathsf{f} = 1$ and the discretization steps are chosen to be small enough to reduce the visible approximation errors. We have applied

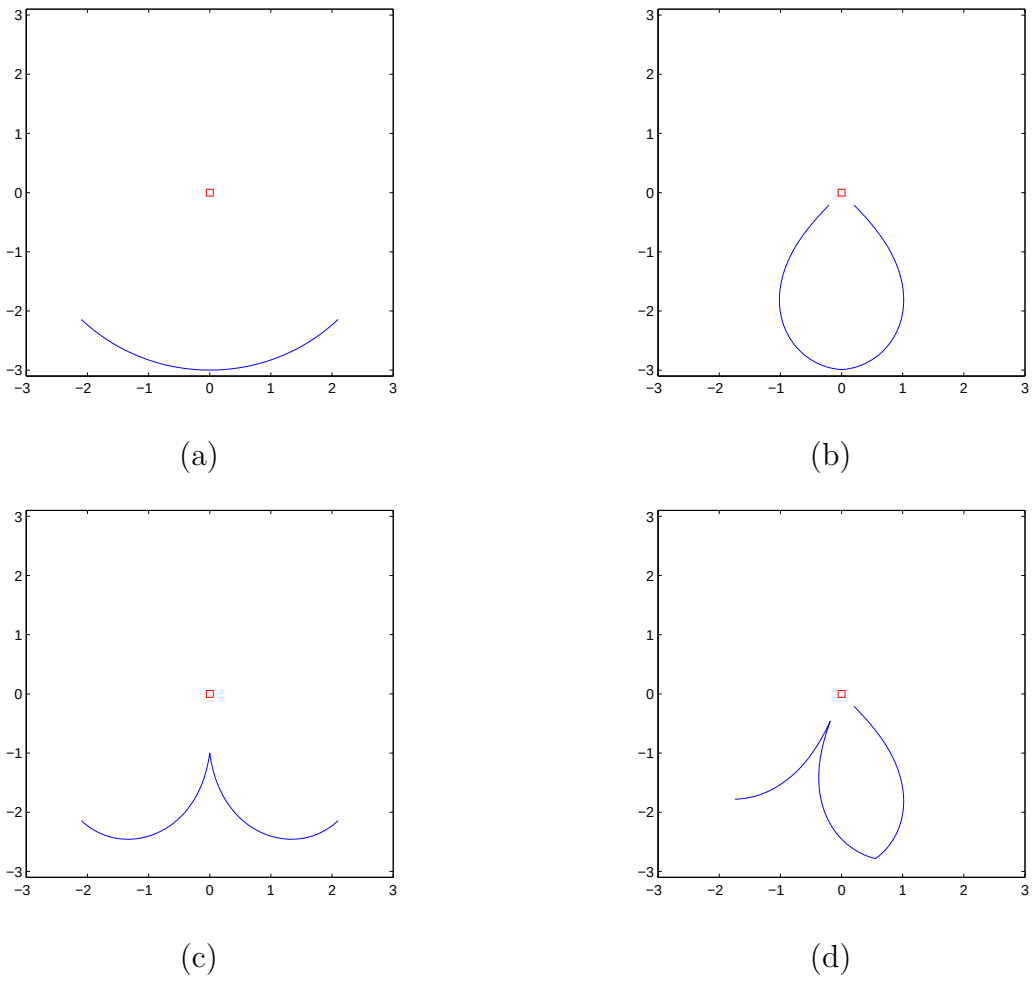

Figure 5: Some reconstructed surfaces with constant brightness function. (a) with state constraints boundary conditions (convergence is reached in one iteration), (b) with Dirichlet boundary conditions, (c) with state constraints boundary conditions and a specific value imposed at the center, and (d) with mixed state constraints and Dirichlet boundary conditions, and a specific value imposed inside the domain. These surfaces can be compared with those in Fig. 2.

state constraint boundary condition. In Figs. 6-7 we present our numerical results.
We see that the first surface is correctly reconstructed in a large part of the domain, and the algorithm fails only near the right-hand boundary. This is expected because the correct value should be carried by a Dirichlet boundary condition, which is not imposed. The second surface is scarcely reconstructed in its shape, but the result is completely wrong if we compare the scales of the figures (the peak is found at $z \approx -6$ while the correct value is $z = -3$). It is useful to note that the example shown in Fig. 7 is rather delicate because the ambiguity is generated by the non-differentiability at a single point. If, for

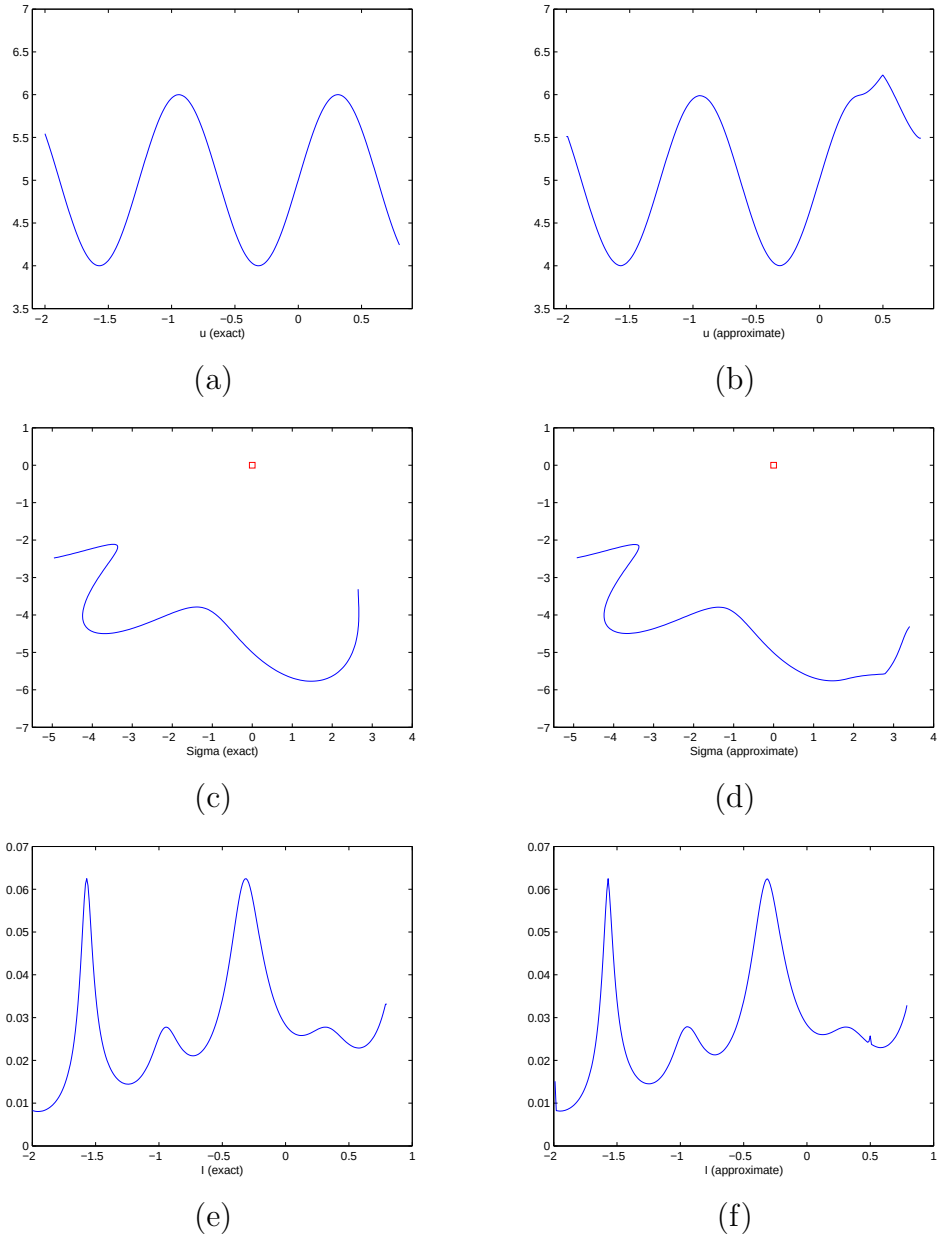

(a) (b) (c) (d) (e) (f)

Figure 6: Numerical outcome for a case similar to that described in Fig. 4-c. First column: exact u, Σ and I. Second column: approximate u, Σ and I.

example, we compute the initial brightness function imposing by hand $u'(0) = 0$ (at the discrete level), the minimal point is detected and the surface is perfectly reconstructed. It is also noticeable that I is well approximated everywhere while this is not true for u, which confirms the existence of an ambiguity.

It should be clear that the generalized concave/convex ambiguity is not limited to one-

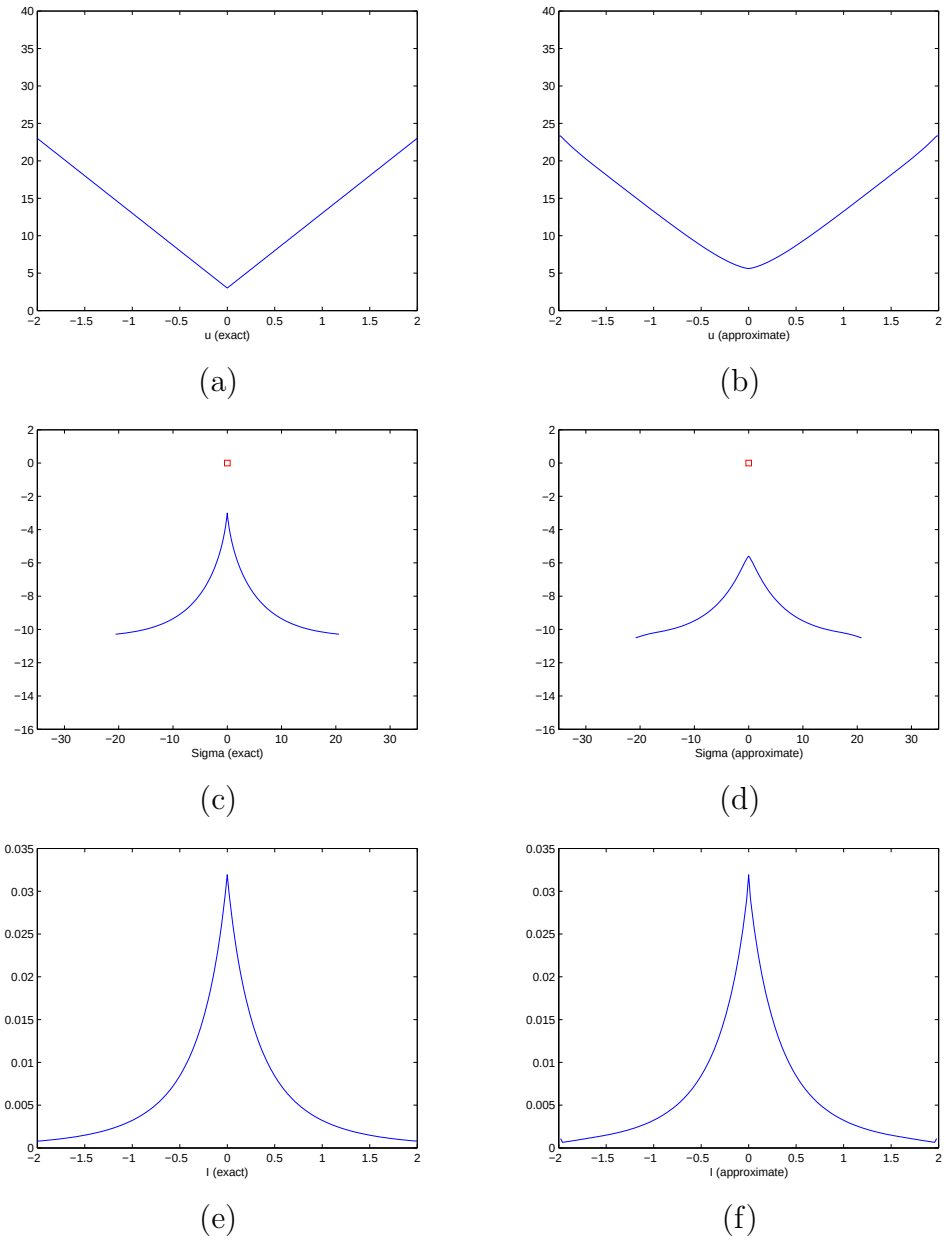

Figure 7: Numerical outcome for a case similar to that described in Fig. 4-d. First column: exact u, Σ and I. Second column: approximate u, Σ and I.

dimensional surfaces. We tried to reconstruct an upside-down pyramid, with Dirichlet boundary condition at the boundary of the base of the pyramid. In Fig. 8 we show the original pyramid as well as the the brightness functions corresponding to (a) the original surface, (b) the reconstructed surface and (c) the surface reconstructed imposing an incorrect value at the center of the image, which forces a peak similar to the one in Fig. 2-f.

As it can be seen, the three images are equal but for a 0-measure set. The differences are

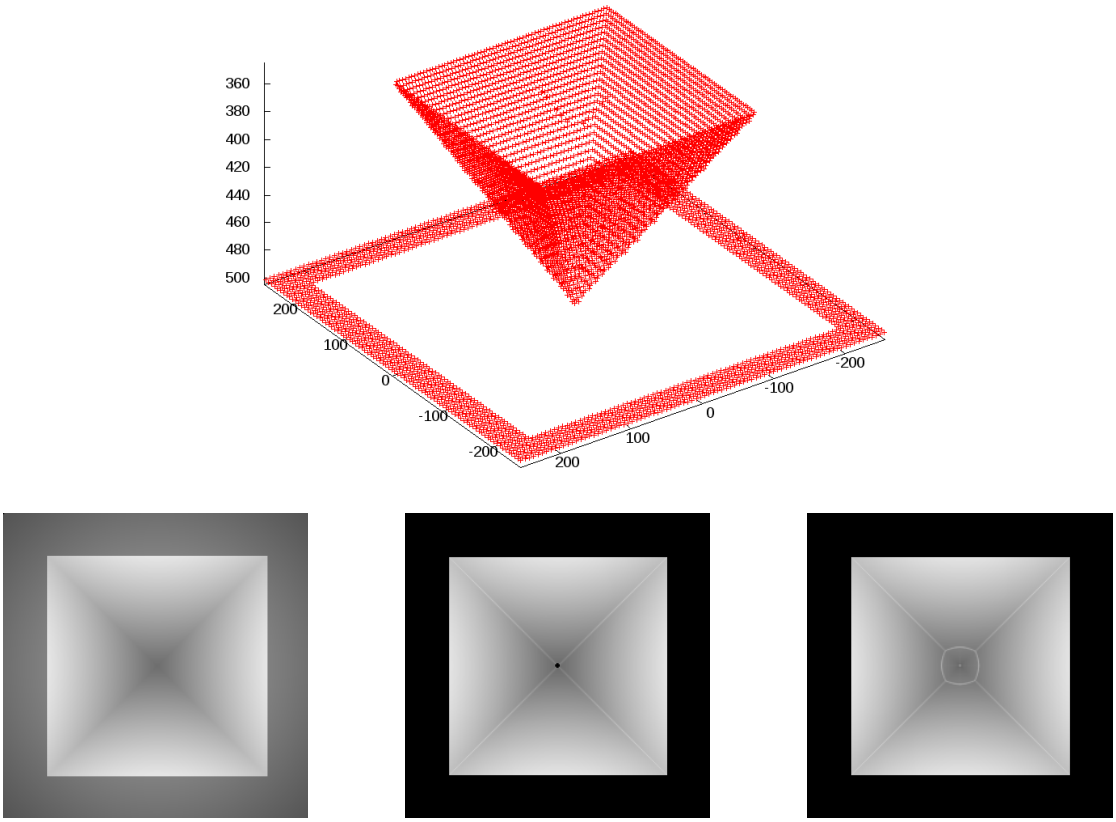

Figure 8: Top: Original upside-down pyramid. Bottom row, from left to right: initial image rendered from the upside-down pyramid, brightness function of the reconstructed surface, and brightness function of the reconstruction where a peak was imposed.

concentrated in the non-differentiable regions and are due to the numerical approximation of the gradient.

4 Two approximation schemes for the PSFS problem

The goal of this section is to analyse two approximation schemes that have been proposed in [33] and [11] (as indicated in the introduction, the two schemes will be referred to by the acronyms VBW and CFS respectively). We will study their analytical properties, and we prove that they converge to the viscosity solution of equation (7). A standard treatment of boundaries is employed for both schemes; we do not mention it explicitly in the text in order to simplify the presentation. We refer the interested reader to [4] for a detailed comparison of the performances of these schemes. Experimental evidence shows that all the

schemes available for the PSFS equation compute comparable solutions, although relevant differences appear in the accuracy and CPU time.

4.1 The VBW scheme: properties and convergence

In this section we describe the VBW scheme, which is the scheme we used in the simulations presented in the previous section. We prove the convergence of the approximate solution to the viscosity solution of equation (7) when the discretization step goes to zero.
In order to simplify the presentation, we first prove the properties of the scheme in one dimension. Then, we will point out how the proofs can be extended to dimension two.

One-dimensional analysis Let us introduce the discretization of spatial derivative made by means of the upwind method as in Rouy and Tourin [29]. Let $\Delta x > 0$ be the spatial mesh width in x direction and denote by $N = N(\Delta x)$ the number of mesh points x_i, $i = 1, \ldots, N$. Denote by w_i the approximate value of v at the i-th mesh point x_i and define $\phi_i(w)$ as

$$\phi_i(w) := \min\left(0, \frac{w_{i+1} - w_i}{\Delta x}, \frac{w_{i-1} - w_i}{\Delta x}\right), \quad \text{for } i = 1, \ldots, N. \tag{27}$$

Then, the approximate gradient is given by

$$\nabla v(x_i) \approx \widetilde{\nabla} w_i := \begin{cases} -\phi_i(w) & \text{if } \phi_i(w) = \frac{w_{i-1} - w_i}{\Delta x}, \\ \phi_i(w) & \text{otherwise.} \end{cases} \tag{28}$$

By the above upwind discretization, one gets the discrete operator

$$L_i(w) := \left(-\frac{I_i}{Q_i}\mathsf{f}^2\sqrt{(\mathsf{f}\widetilde{\nabla} w_i)^2 + (x_i\widetilde{\nabla} w_i)^2 + Q_i^2} + e^{-2w_i}\right), \tag{29}$$

and can write the discrete version of equation (7) as

$$L_i(w) = 0, \quad \text{for } i = 1, \ldots, N. \tag{30}$$

Introducing the parameter $\tau > 0$, we obtain the fixed point form:

$$w = G^\tau(w), \tag{31}$$

simply defining G^τ componentwise by

$$G_i^\tau(w) := w_i + \tau L_i(w), \qquad i = 1, \ldots N. \tag{32}$$

We describe important structural properties of the scheme in the following proposition.

Proposition 4.1 *Let $G^\tau : \mathbb{R}^N \to \mathbb{R}^N$ be defined as in* (32). *The following properties hold true:*
(i) there exists $\tau^* > 0$ such that $w_1 \le w_2$ implies $G^\tau(w_1) \le G^\tau(w_2)$ for $\tau < \tau^*$;
(ii) if $\tau < \tau^*$, then

$$\|G^\tau(w_1) - G^\tau(w_2)\|_\infty < \|w_1 - w_2\|_\infty, \text{ for any } w_1, w_2 \in \mathbb{R}^N.$$

Proof Let us first assume that the evaluation of (28) gives $\widetilde{\nabla} w_i = \frac{w_i - w_{i-1}}{\Delta x}$, which implies $w_i - w_{i-1} > 0$. Then, we have

$$\frac{\partial G_i^\tau(w)}{\partial w_i} = 1 - \frac{\tau I_i \mathsf{f}^2}{Q_i} \frac{(x_i^2 + \mathsf{f}^2)\frac{w_i - w_{i-1}}{\Delta x^2}}{\sqrt{(\mathsf{f}^2 + x_i^2)\left(\frac{w_i - w_{i-1}}{\Delta x}\right)^2 + Q_i^2}} - 2\tau e^{-2w_i}\,, \tag{33}$$

$$\frac{\partial G_i^\tau(w)}{\partial w_{i-1}} = \frac{\tau I_i \mathsf{f}^2}{Q_i} \frac{(x_i^2 + \mathsf{f}^2)\frac{w_i - w_{i-1}}{\Delta x^2}}{\sqrt{(\mathsf{f}^2 + x_i^2)\left(\frac{w_i - w_{i-1}}{\Delta x}\right)^2 + Q_i^2}} \tag{34}$$

and

$$\frac{\partial G_i^\tau(w)}{\partial w_{i+1}} = 0. \tag{35}$$

The term $\partial G_i^\tau(w)/\partial w_{i-1}$ is always positive, whereas $\partial G_i^\tau(w)/\partial w_i$ is positive only for τ sufficiently small. Note that the maximal value τ^* can be explicitly computed by means of (33), and the condition $\tau < \tau^*$ can be explicitly verified while the algorithm is running. If $\widetilde{\nabla} w_i = \frac{w_{i+1} - w_i}{\Delta x}$ we get a similar result. Let us assume now that $\widetilde{\nabla} w_i = 0$. We get

$$G_i^\tau(w) = w_i - \tau I_i \mathsf{f}^2 + \tau e^{-2w_i}$$

and then

$$\frac{\partial G_i^\tau(w)}{\partial w_i} = 1 - 2\tau e^{-2w_i}\,, \quad \frac{\partial G_i^\tau(w)}{\partial w_{i-1}} = \frac{\partial G_i^\tau(w)}{\partial w_{i+1}} = 0.$$

Again, the three terms are positive provided τ is sufficiently small. This proves (i).
Let us denote by J_{G^τ} the Jacobian matrix of G^τ. Whatever the evaluation of $\widetilde{\nabla} w$ gives, assuming that τ is sufficiently small, we get

$$\|J_{G^\tau}\|_\infty = \max_i \left\{ \frac{\partial G_i^\tau}{\partial w_{i-1}} + \frac{\partial G_i^\tau}{\partial w_i} + \frac{\partial G_i^\tau}{\partial w_{i+1}} \right\} = \max_i \left\{ 1 - 2\tau e^{-2w_i} \right\}\,, \tag{36}$$

which is always strictly lower than 1 and this ends the proof. ♣

The algorithm is implemented in the fixed point form, i.e.

$$w_i^{(n+1)} = G_i^\tau(w^{(n)})\,, \qquad i = 1, \dots N\,, \quad n = 0, 1, \dots \tag{37}$$

with $w^{(0)}$ as in (26).

Proposition 4.2 *Let $w^{(0)}$ be chosen as in* (26) *and let τ be sufficiently small. Then,*
(i) the algorithm (37) *converges to the unique fixed point $\widehat{w}^{\Delta x,\tau}$, and*
(ii) $w_i^{(n+1)} \leq w_i^{(n)}$ for any i and any n.

Proof In order to apply the fixed point theorem, we only have to show that $G^\tau : X \to X$, where X is a compact subset of $\mathbb{R}^N$. Given the set-up of the experiment, it is easy to restrict the range of the function v (which depends on the function r) finding two values $w_{\min}$ and $w_{\max}$ such that $w_{\min} \leq v \leq w_{\max}$. A natural choice is then $X = [w_{\min}, w_{\max}]^N$. In the following the right choice of $w_{\max}$ will be detailed more precisely. Let us fix $w \in X$ and $i \in \{1, \dots, N\}$. The proof is divided in two steps:
(a) We prove that $G_i^\tau(w) \geq w_{\min}$. If $w_i = w_{\min}$, the neighbouring nodes of x_i cannot have a smaller value than w_i, then the evaluation of $\widetilde{\nabla} w_i$ gives $\widetilde{\nabla} w_i = 0$. Moreover, $w_{\min}$ is by definition smaller than the exact value $v(x_i)$. Then we have

$$G_i^\tau(w) = w_{\min} + \tau \left(-\frac{I_i \mathsf{f}^2}{Q_i} \sqrt{0 + 0 + Q_i^2} + e^{-2w_{\min}} \right) \geq w_{\min} + \tau \left(-I_i \mathsf{f}^2 + e^{-2v(x_i)} \right) \geq$$
$$w_{\min} + \tau \left(-\frac{I_i \mathsf{f}^2}{Q_i} \sqrt{(\mathsf{f} \nabla v_i)^2 + (x_i \nabla v_i)^2 + Q_i^2} + e^{-2v(x_i)} \right) = w_{\min} + \tau \cdot 0 = w_{\min}.$$

If $w_i > w_{\min}$, we have $G_i^\tau(w) = w_i + \tau L_i(w)$. The result is obtained choosing τ in such a way that

$$\tau |L_i(w)| \leq w_i - w_{\min}. \tag{38}$$

(b) Let us now prove that $G_i^\tau(w) \leq w_{\max}$. If $w_i = w_{\max}$, we have

$$G_i^\tau(w) = w_{\max} + \tau \left(-\frac{I_i \mathsf{f}^2}{Q_i} \sqrt{(\mathsf{f} \widetilde{\nabla} w_i)^2 + (x_i \widetilde{\nabla} w_i)^2 + Q_i^2} + e^{-2w_{\max}} \right).$$

Since $Q_i < +\infty$ and we assume that $I_i > 0$, the desired result follows choosing $w_{\max}$ sufficiently large, so that the term $e^{-2w_{\max}}$ is small enough the the negative term be leading. If instead $w_i < w_{\max}$, the result is obtained similarly to before, choosing τ in such a way that

$$\tau |L_i(w)| \leq w_{\max} - w_i. \tag{39}$$

We can now apply the fixed point theorem and conclude that (i) holds true. *A posteriori*, we realize that conditions (38)-(39) are not really restrictive, since convergence to the fixed point implies that $L(w^{(n)}) \to 0$ for $n \to +\infty$.
The choice of the initial guess is the key property to obtain monotone decreasing convergence to the fixed point. In fact, $w^{(0)}$ is larger (or equal) than the solution (see Section 3.2) and G^τ verifies Proposition 4.1-(i). This proves (ii). ♣

We want to prove convergence of the numerical solution $\widehat{w}^{\Delta x,\tau}$ to the viscosity solution v of the equation (7), for $\Delta x \to 0$. We can rely on the classic results of Barles and Souganidis [1], following the same strategy of Rouy and Tourin [29].

Proposition 4.3 *Let $w^{(0)}$ be chosen as in* (26) *and let $\tau^* = \tau^*(\Delta x)$ be the "constant" defined by Proposition 4.1. If $\tau(\Delta x) < \tau^*(\Delta x)$, then $\widehat{w}^{\Delta x,\tau(\Delta x)}$ converges locally uniformly to v for $\Delta x \to 0$.*

Proof We start proving that the scheme is monotone in the sense given in [1]. We know that the fixed point $\widehat{w}^{\Delta x,\tau}$ satisfies the equation

$$L(w) = 0\,,$$

so we will use this form, since in [1] the discrete operator is written in the implicit form $S(h, x, w(x), w) = 0$, where $S : \mathbb{R}^+ \times \overline{\Omega} \times \mathbb{R} \times B(\overline{\Omega}) \to \mathbb{R}$ and $B(\overline{\Omega})$ is the space of bounded functions defined on $\overline{\Omega}$. If the evaluation of (28) gives $\widetilde{\nabla} w_i = \frac{w_i - w_{i-1}}{\Delta x}$, we only have to prove that $\frac{\partial L_i(w)}{\partial w_{i-1}}$ does not change sign. By (34) we easily get $\frac{\partial L_i(w)}{\partial w_{i-1}} > 0$. If the evaluation of (28) gives $\widetilde{\nabla} w_i = \frac{w_{i+1} - w_i}{\Delta x}$ we obtain analogously $\frac{\partial L_i(w)}{\partial w_{i+1}} > 0$. Finally, if $\widetilde{\nabla} w_i = 0$, L_i does not depend on w_{i-1} nor w_{i+1}.
The *stability* and *consistency* of the scheme are easy to prove. Since the *comparison principle* for the problem is proven in [28] we know that the equation (7) has a unique viscosity solution v and we can conclude, by the general convergence result in [1], that the approximate solution converges locally uniformly to v. ♣

It is interesting to note that the property pointed out in Proposition 3.1 is preserved in the numerical approximation. Let us assume that the assumptions of Proposition 4.3 are satisfied. We want to show that

$$\begin{cases} w_i^{(n+1)} > w_{i-1}^{(n)} & \text{if } \widetilde{\nabla} w_i = \frac{w_i - w_{i-1}}{\Delta x}\,, \\ w_i^{(n+1)} > w_{i+1}^{(n)} & \text{if } \widetilde{\nabla} w_i = \frac{w_{i+1} - w_i}{\Delta x}\,, \\ w_i^{(n+1)} = w_i^{(n)} & \text{if } \widetilde{\nabla} w_i = 0. \end{cases} \tag{40}$$

If (40) holds, the solution is constructed from the smallest to the largest values, and then the solution cannot become lower than the information sources (Dirichlet boundary conditions or minimum points automatically detected). Let us prove the first line in (40). To this end, we first recall that

$$w_i^{(n+1)} = G_i(w^{(n)}) = w_i^{(n)} + \tau L_i(w^{(n)}).$$

Note that Proposition 4.2-(*ii*) implies $L_i(w^{(n)}) < 0$ for any i and n. In order to have $w_i^{(n+1)} > w_{i-1}^{(n)}$ the parameter τ must be chosen in such a way that

$$\tau |L(w^{(n)})| < (w_i^{(n)} - w_{i-1}^{(n)})$$

which corresponds to

$$\tau < \frac{w_i^{(n)} - w_{i-1}^{(n)}}{-L_i(w^{(n)})}. \tag{41}$$

Note that the right-hand term in (41) is strictly positive. For any fixed Δx, the term $L_i(w^{(n)})$ tends to zero when n tends to infinity (this follows by the fact that the algorithm converges to the fixed point). Then, the condition (41) is always satisfied in the limit.
We can also obtain the results similar to those proven for the continuous model. Let us write

$$\frac{w_i^{(n+1)} - w_{i-1}^{(n)}}{\Delta x} = \frac{w_i^{(n+1)} - w_i^{(n)}}{\Delta x} + \frac{w_i^{(n)} - w_{i-1}^{(n)}}{\Delta x}.$$

Since, as we have just seen, $w_i^{(n+1)} - w_{i-1}^{(n)} \geq 0$ and we know that $w_i^{(n+1)} - w_i^{(n)} \leq 0$ (because the algorithm computes a decreasing sequence), we obtain that $w_i^{(n)} - w_{i-1}^{(n)} \geq 0$ for any Δx, and then, passing to the limit (in the case it exists),

$$\lim_{\Delta x \to 0^+} \frac{w(x_i) - w(x_i - \Delta x)}{\Delta x} \geq 0\,,$$

which corresponds to the fact that the solution is increasing along the characteristic direction.

Two-dimensional analysis While the ambiguity issues can be investigated in one dimension without loss of generality, real-world applications of (P)SFS require a two-dimensional approach. The strategy developed in the one-dimensional case can be easily generalized, and all the main results still hold. The only difference is a new condition on the experimental set-up which is necessary to prove that $w_1 \leq w_2$ implies $G^\tau(w_1) \leq G^\tau(w_2)$.
Assuming a square uniform $N \times N$ grid with $\Delta x = \Delta y$, the scheme is now defined componentwise by

$$G^\tau_{i,j}(w) := w_{i,j} + \tau L_{i,j}(w)\,, \qquad i,j = 1, \dots N \tag{42}$$

where

$$L_{i,j}(w) := \tag{43}$$
$$-\frac{I_{i,j}}{Q_{i,j}}\mathsf{f}^2\sqrt{\mathsf{f}^2\left((\widetilde{\nabla}_x w_{i,j})^2 + (\widetilde{\nabla}_y w_{i,j})^2\right) + (x_i\widetilde{\nabla}_x w_{i,j} + y_j\widetilde{\nabla}_y w_{i,j})^2 + Q_{i,j}^2} + e^{-2w_{i,j}}.$$

Let us assume that $\widetilde{\nabla} w_{i,j}$ is evaluated by $\frac{1}{\Delta x}\,(w_{i,j} - w_{i-1,j}, w_{i,j} - w_{i,j-1})$.

$$\frac{\partial G^\tau_{i,j}(w)}{\partial w_{i-1,j}} = \frac{\tau I_{i,j}\mathsf{f}^2}{Q_{i,j}}\frac{A_{ij}(w)}{\sqrt{B_{ij}(w)}} \tag{44}$$

where

$$A_{ij}(w) := (x_i^2 + \mathsf{f}^2)\frac{w_{i,j} - w_{i-1,j}}{\Delta x^2} + x_i y_j \frac{w_{i,j} - w_{i,j-1}}{\Delta x^2} \tag{45}$$

$$\begin{aligned} B_{ij}(w) : \;&=\; \mathsf{f}^2\left(\frac{w_{i,j} - w_{i-1,j}}{\Delta x}\right)^2 + \mathsf{f}^2\left(\frac{w_{i,j} - w_{i,j-1}}{\Delta x}\right)^2 + \\ &+\; \left(x_i\frac{w_{i,j} - w_{i-1,j}}{\Delta x} + y_j\frac{w_{i,j} - w_{i,j-1}}{\Delta x}\right)^2 + Q_{i,j}^2 \end{aligned} \tag{46}$$

and an analogous result for $\partial G^{\tau}_{i,j}(w)/\partial w_{i,j-1}$. With no further assumptions, the quantity in (44) can be negative, due to the term $x_i y_j$ in (45), which has no fixed sign. Then, in order to get the same result as in the one-dimensional case, namely $\|J_{G^\tau}\|_\infty = \max_{i,j}\{1 - 2\tau e^{-2w_{i,j}}\}$, we need to assume that

$$(x_i^2 + \mathsf{f}^2)\,(w_{i,j} - w_{i-1,j}) + x_i y_j\,(w_{i,j} - w_{i,j-1}) \geq 0 \tag{47}$$

and, analogously, that

$$(y_j^2 + \mathsf{f}^2)\,(w_{i,j} - w_{i,j-1}) + x_i y_j\,(w_{i,j} - w_{i-1,j}) \geq 0. \tag{48}$$

As the conditions (47)-(48) incorporate a coupling of image dimension and focal length, they imply a condition on the experimental set-up. They are fulfilled if f is sufficiently large, or if the surface is fully contained in the "positive" region $\{x > 0,\ y > 0\}$.

4.2 The CFS scheme: properties and convergence

In order to simplify the notations, let us prove the result in the one-dimensional case. Generalization to higher dimension is trivial and all the results are preserved. The semi-discrete formulation of the CFS scheme was derived in [10, 11], we report it here for the reader's convenience. For any function $w : \mathbb{R} \to \mathbb{R}$, we define the semi-discrete operator F^h as

$$F^h[w](x) := \min_{a \in \overline{B(0,1)}} \{w(x + hb(x,a)) + h\ell(x,a)\} + he^{-2w(x)}. \tag{49}$$

The iterative algorithm can be written in compact form as

$$\begin{cases} w^{(n+1)}(x) = F^h[w^{(n)}](x)\,, \quad n = 0, 1, \dots \\ w^{(0)}(x) = -\frac{1}{2}\ln(I(x)\mathsf{f}^2). \end{cases} \tag{50}$$

As usual, the parameter h must be intended as a fictitious-time discretization step used to integrate along characteristics in the semi-Lagrangian formulation. We do not consider here the fully-discrete problem in which the operator F^h is projected on a grid.
In the following we prove that the sequence generated by the algorithm (50) actually converges to some function w^h. Note that we employ here a different approach than the one used in the previous subsection for the analysis of the VBW method. More precisely, we will *not* prove that the operator F^h is a contraction mapping, but we prove that the sequence $\{w^{(n)}\}_{n\geq 0}$ is monotone decreasing and bounded from below.

Proposition 4.4 (boundedness from below) *Let $w \in C^0(\Omega)$. For any $x \in \Omega$ there exists a step $h = h(x) > 0$ and a constant $w_{\min} \in \mathbb{R}$ such that*

$$w(x) \geq w_{\min} \text{ implies } F^h[w](x) \geq w_{\min}. \tag{51}$$

Proof Let us consider separately two cases.
i) Let $w(x) = w_{\min}$. We first note, by the definition of l in (11), that $\ell(x,0) = \min_a\{\ell(x,a)\}$.

Second, by the definition of b in (11), we have $w(x + hb(x, 0)) = w(x) = \min_a\{w(x + hb(x, a))\}$ since the minimum of w is attained at x by assumption. As a consequence, the minimum in (49) is attained for $a^* = 0$. Then,

$$F^h[w](x) = w(x) - hI(x)\mathsf{f}^2 + he^{-2w(x)} = w_{\min} + h\left(e^{-2w_{\min}} - I(x)\mathsf{f}^2\right).$$

For $w_{\min}$ sufficiently small, we get

$$e^{-2w_{\min}} - I(x)\mathsf{f}^2 \geq 0$$

and then $F^h[w](x) \geq w_{\min}$. Note that it is possible to choose a suitable $w_{\min}$ uniformly in x. To this end, it is sufficient to choose $w_{\min} \leq \min_{x\in\Omega} w^{(0)}(x)$.

(ii) Let $w(x) > w_{\min}$. The continuity of w guarantees that there exists a ball $B(x, \xi)$ centred in x of radius ξ such that $w(x') > w_{\min}$ for every $x' \in B(x, \xi)$. Let us denote by a^* the $\arg\min$ appearing in the definition of $F^h[w]$. Defining $\Delta w = w(x + hb(x, a^*)) - w_{\min}$, we have

$$\begin{aligned} F^h[w](x) &= w(x + hb(x, a^*)) + h\ell(x, a^*) + he^{-2w(x)} \\ &= w_{\min} + \Delta w + h(e^{-2w(x)} + \ell(x, a^*)) \\ &\geq w_{\min} + \Delta w + h(0 - I(x)\mathsf{f}^2). \end{aligned}$$

Choosing h in such a way that $h \max_a b(x, a) < \xi$, we have $\Delta w > 0$. Moreover, we note that Δw does not tend to zero if h tends to zero. The conclusion follows by choosing $h \leq \Delta w / I(x)\mathsf{f}^2$. ♣

Proposition 4.5 (monotonicity) *Let us assume that $w^{(n)} \in C^1(\Omega)$ for any $n \in \mathbb{N}$. Then, for any $n \in \mathbb{N}$ there exists a step $h = h(n) > 0$ such that the sequence defined in (50) verifies*

$$w^{(n+1)}(x) \leq w^{(n)}(x) \quad \textit{for any } x \in \Omega.$$

Proof We first consider points x such that the corresponding a^* is equal to zero at the first iteration $n = 0$. These are the points where the initial guess $w^{(0)}$ is actually the correct solution, see Section 3.2. In this case we have

$$w^{(1)}(x) = w^{(0)}(x) - hI(x)\mathsf{f}^2 + he^{-2w^{(0)}(x)} = w^{(0)}(x).$$

Since the solution already reached convergence at these points, we can simply stop the computation (so that $w^{(n+1)}(x) = w^{(n)}(x)$ for any n).
Let us now consider a point x such that $a^*(x) \neq 0$ for $n = 0$. We prove the assertion by induction on n. We have

$$w^{(1)}(x) = w^{(0)}(x + hb(x, a^*)) + h\ell(x, a^*) + he^{-2w^{(0)}(x)}.$$

Since $a^* \neq 0$, we have

$$w^{(0)}(x + hb(x, a^*)) + h\ell(x, a^*) < w^{(0)}(x + hb(x, 0)) + h\ell(x, 0) = w^{(0)}(x) - hI(x)\mathsf{f}^2 \quad (52)$$

and then $w^{(1)}(x) < w^{(0)}(x) - hI(x)\mathsf{f}^2 + he^{-2w^{(0)}(x)} = w^{(0)}(x)$. Note that we could find two different optimal controls $a_1^* = 0$ and $a_2^* \neq 0$ in which the minimum is attained, so that the strict inequality in (52) does not hold true. This issue can be fixed assuming that in such an ambiguous case we keep a_1^* as optimal control.

Now we prove that

$$w^{(n)}(x) < w^{(n-1)}(x) \text{ implies } w^{(n+1)}(x) < w^{(n)}(x).$$

We have to prove that $F^h[w^{(n)}](x) < F^h[w^{(n-1)}](x)$. Let us denote by a^* the $\arg\min$ for $F^h[w^{(n-1)}](x)$. Note that a^* is in general different from the minimizing choice for $F^h[w^{(n)}](x)$). Then it is sufficient to show that

$$\begin{aligned} &w^{(n)}(x + hb(x, a^*)) + h\ell(x, a^*) + he^{-2w^{(n)}(x)} \\ &< w^{(n-1)}(x + hb(x, a^*)) + h\ell(x, a^*) + he^{-2w^{(n-1)}(x)} \end{aligned}$$

or, analogously, that

$$w^{(n)}(x + hb(x, a^*)) - w^{(n-1)}(x + hb(x, a^*)) + h\Big(e^{-2w^{(n)}(x)} - e^{-2w^{(n-1)}(x)}\Big) < 0.$$

Since the function $z \mapsto e^{-2z}$ is differentiable and $w^{(n)}(x) \geq w_{\min}$ for any n (see Prop. 4.4), we have

$$\Big(e^{-2w^{(n)}(x)} - e^{-2w^{(n-1)}(x)}\Big) < 2e^{-2w_{\min}}\Big(w^{(n-1)}(x) - w^{(n)}(x)\Big).$$

Then, we only need to prove that

$$w^{(n)}(x + hb(x, a^*)) - w^{(n-1)}(x + hb(x, a^*)) + 2he^{-2w_{\min}}\Big(w^{(n-1)}(x) - w^{(n)}(x)\Big) < 0.$$

Let us define $C := 2e^{-2w_{\min}}$ and use the first-order Taylor series expansion for $w^{(n)}$ and $w^{(n-1)}$. We have

$$\begin{aligned} &(1 - Ch)w^{(n)}(x) + (Ch - 1)w^{(n-1)}(x) + \\ &+hb(x, a^*) \cdot \Big(\nabla w^{(n)}(x) - \nabla w^{(n-1)}(x)\Big) + O(h^2) < 0. \end{aligned} \quad (53)$$

When h tends to zero, the left hand side of the previous inequality tends to $w^{(n)}(x) - w^{(n-1)}(x)$, which is strictly negative by assumption. Then there exists a h sufficiently small such that (53) holds true. ♣

To conclude, let us observe that assuming $I \in C^1(\Omega)$, we have $w^{(0)} \in C^1(\Omega)$ and then $w^{(n)} \in C^1(\Omega)$ for any n, since the regularity is preserved by the operator F^h. Under this assumption, the two previous propositions can be applied, and we get the convergence of the sequence defined in (50).
Finally, note that the dependence of the step h on x and n is not an issue in the implementation of the numerical approximation because the space is discretized in a finite number of nodes and the algorithm is stopped after a finite number of iterations.

5 Overcoming the ambiguity

In this section we suggest a simple algorithm to overcome the ambiguity issue in some cases. In particular, we try to reconstruct *discontinuous surfaces*. Numerical tests performed in [4, 10, 11] clearly show that the PSFS algorithm is not able to catch discontinuities of the surface. In fact, it tries to reconstruct a continuous surface with the same brightness function as the original one. In order to deal with discontinuities, the idea is to perform first a segmentation of the input image, dividing the domain into several subdomains. The boundaries of the subdomains correspond to the curves of discontinuity of the brightness function. Then, we apply the PSFS algorithm piecewise in every subdomain where the brightness function is continuous. For each subdomain, initial data for the iterative schemes are computed as in (25).
The question arises which boundary conditions have to be imposed at the boundary of each subdomain. In the following we impose always state constraints boundary conditions there.

Synthetic input data We test the new algorithm on a synthetic photograph of an upside-down pyramid over a flat surface. See Fig. 9-a,b for the input photograph and the true surface (the surface is reversed for visualization purposes).
Applying directly the PSFS algorithm, we obtain the surface depicted in Fig. 9-c, where the discontinuity is totally lost. Note that the reconstructed surface has the same brightness function as the original one. It is also worth to note that only the pyramid is well reconstructed.
Applying the PSFS algorithm after the segmentation, we face to solve two separate problems (for the pyramid and for the frame). The result is shown in 9-d. This time the flat surface is correctly reconstructed too, showing that our procedure works. For the experiment, we used a 256×256 grid and $\mathsf{f} = 250$. The reconstruction errors (depth error compared to the ground truth) are summarized in Table 1.

Table 1: Errors for the test described in Section 5.

Algorithm	L^1 error	L^∞ error
Direct	8.74%	26.71%
Segmented	2.55%	4.80%

Real-world input data Our aim is now to show that the strategy to employ state constraints boundary conditions at object boundaries works favourably, as in the synthetic pyramid test.
As an example of an image for real-world data we consider the image at the top in Fig. 10. The image was acquired with a Nikon D90 camera, and it has been downsampled to

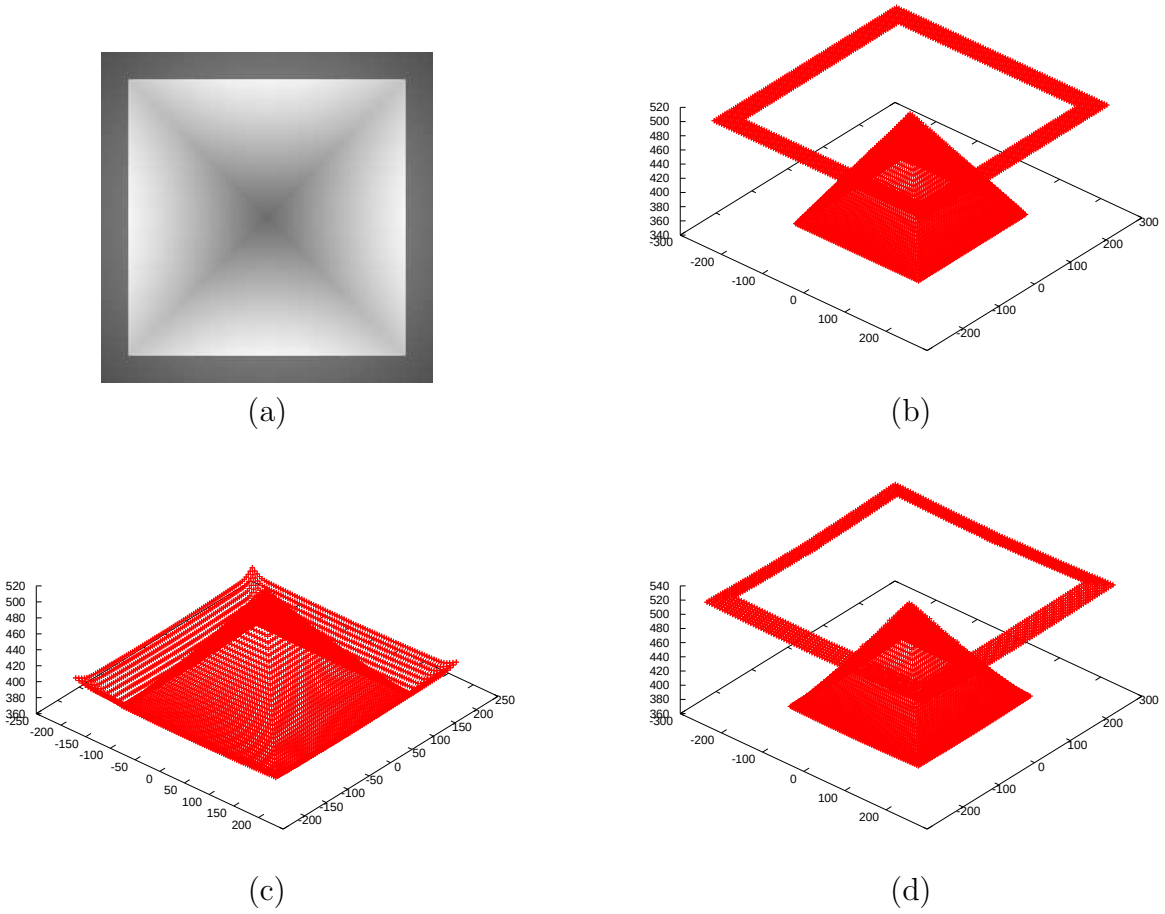

Figure 9: (a) Input image, (b) input surface (reversed), (c) reconstructed surface by a direct application of the PSFS scheme (state constraint b.c.), (d) reconstructed surface after segmentation (state constraint b.c.).

800×531 pixels. The focal length in multiples of the resulting pixel size is 1525. As usual for real-world imges, the reflectance and lighting parameters need to be estimated by us. We employed the following numbers for the σ: 100000 for the background, 73000 for the blue mug, and 110000 for the beige cup.

The segment borders separating the cup from the mug as well as those separating cup/mug from background, were obtained here by hand. They were enhanced a bit in order to mask out points where interreflections between the objects are very strong. The specular highlight at the upper lip of the cup was also masked out since such specular reflections are not included in our PSFS model. At the three resulting segments – cup, mug and background – the PSFS equation was applied separately under state constraints boundary conditions.

Let us turn to the corresponding experimental result, see Fig. 10 (bottom). The general

shape of the objects and the background is captured in a rather accurate way. As expected, there is no visible tendency to enforce continuous transition zones between the segments. This shows that the proposed idea to use state constraint boundary conditions at the borders of segmented objects works properly.
Concerning the quality of results we observe some artefacts, as expected for this relatively difficult real-world input image. The cup is reflected on the surface of the mug, and in addition there are a lot of specular reflections as by the rough surface of the mug, so that its reconstruction is drawn towards the camera. Both cup and mug are reflected on the green cardboard of the background, so that the latter is not reconstructed perfectly flat. We also chose not to display the reconstruction of the ground the cup/mug are standing on, since the absence of critical points there leads to a misinterpretation of the depth. The underlying modelling assumptions are violated here: Objects should have at least one point where the surface normal points to the camera and where the distance to it is minimal. Moreover, the quality of the reconstruction of the ground is degraded since the reflections of both the cup and the mug are strongly visible there.

Conclusion

In this paper, we have extensively studied analytically and numerically the PSFS model and the related Hamilton-Jacobi equation.
It turns out that a generalized concave/convex ambiguity can still arise in the model as well as in practical computations. This is particularly important at points where the sought surface is not differentiable. A way to circumvent this difficulty is proposed here: We combine PSFS with a segmentation step and state constraints boundary conditions at the segment borders.
We have also proved the convergence of a finite-difference and a semi-Lagrangian numerical scheme for the PSFS equation. In the latter case we employed an innovative technique for the proof that can be useful also in other contexts than PSFS. Our theoretical results support the previous investigation about the generalized concave/convex ambiguity, assuring that the ambiguity issues are not due to numerical artefacts. Finally, we have validated with these schemes the currently most important iterative solvers for PSFS.
Modern models like the PSFS model studied here have a significant potential for applications. We believe that this paper represents an important step towards a deeper understanding of PSFS and other state-of-the-art SFS models as well as towards the use of mathematically established numerical techniques in modern computer vision.

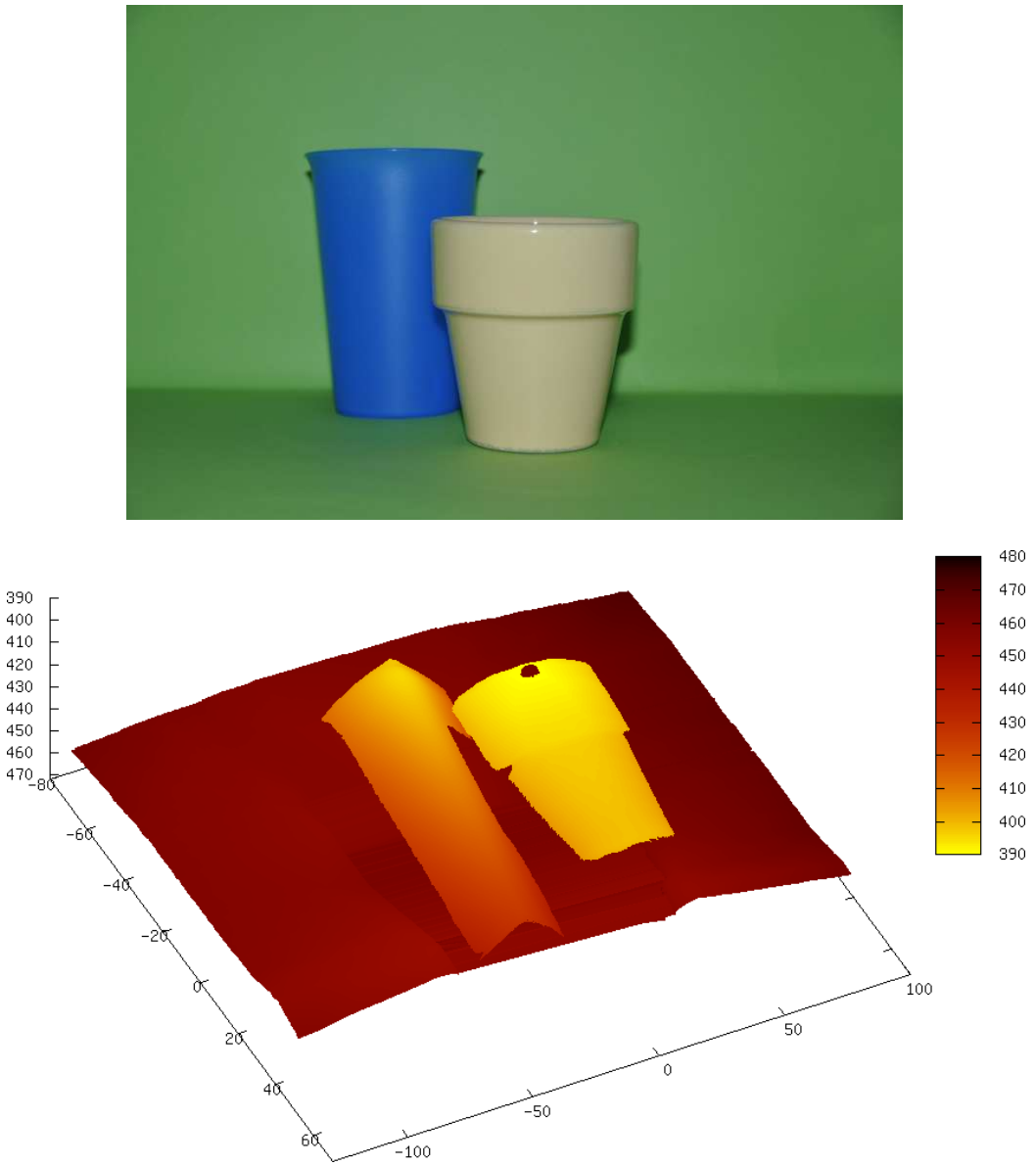

Figure 10: Real-world input image (top) and 3-D reconstruction (bottom).

A Derivation of PSFS equation in Cartesian coordinates

Starting from (1) and (2), we have (see Figure 1):

$$M(x,y) = \frac{\mathsf{f}u(x,y)}{d(x,y)} \begin{pmatrix} x \\ y \\ -\mathsf{f} \end{pmatrix},$$

where:

$$d(x,y) = \sqrt{x^2 + y^2 + \mathsf{f}^2}.$$

The two vectors $\partial_x M$ and $\partial_y M$ form a basis in the plane orthogonal to the normal direction $\widehat{n}(x,y)$ at the point $M = M(x,y)$. We have

$$\partial_x M = \frac{\mathsf{f}}{d^3}\left(d^2u + d^2xu - x^2u, y(d^2u_x - xu), \mathsf{f}(-d^2u_x + xu)\right)^\top,$$
$$\partial_y M = \frac{\mathsf{f}}{d^3}\left(x(d^2u_y - yu), d^2u + d^2yu_y - y^2u, \mathsf{f}(-d^2u_y + yu)\right)^\top.$$

After some algebra, we find

$$\partial_x M \times \partial_y M = \frac{\mathsf{f}^2 u}{d^2}\left(\mathsf{f}\left(u_x - \frac{xu}{d^2}\right), \mathsf{f}\left(u_y - \frac{yu}{d^2}\right), \frac{\mathsf{f}^2 u}{d^2} + xu_x + yu_y)\right)^\top,$$

which, after a normalization, gives

$$\widehat{n}(x,y) = \frac{\pm 1}{\sqrt{\mathsf{f}^2\|\nabla u\|^2 + (\nabla u \cdot (x,y))^2 + (\mathsf{f}u/d)^2}} \begin{pmatrix} \mathsf{f}(u_x - xu/d^2) \\ \mathsf{f}(u_y - yu/d^2) \\ \dfrac{\mathsf{f}^2 u}{d^2} + \nabla u \cdot (x,y) \end{pmatrix}. \tag{54}$$

Knowing that in each visible point M the normal $\widehat{n}$ points towards C, it follows that the right sign in (54) is equal to $+$, so we get from (54) and (4):

$$\omega(x,y) \cdot \widehat{n}(x,y) = \frac{\mathsf{f}u}{d\sqrt{\mathsf{f}^2\|\nabla u\|^2 + (\nabla u \cdot (x,y))^2 + (\mathsf{f}u/d)^2}}.$$

In conclusion, knowing that $r = \mathsf{f}\,u$, Equation (6) can be written as:

$$d\mathsf{f}u\sqrt{\mathsf{f}^2\|\nabla u\|^2 + (\nabla u \cdot (x,y))^2 + (\mathsf{f}u/d)^2} = \frac{1}{I},$$

or, using the change in the unknown $v = \ln(u)$:

$$Id\mathsf{f}\sqrt{\mathsf{f}^2\|\nabla v\|^2 + (\nabla v \cdot (x,y))^2 + (\mathsf{f}/d)^2} = e^{-2v}, \tag{55}$$

which easily gives the Hamilton-Jacobi equation (7), since $Q = \mathsf{f}/d$.

B Derivation of PSFS equation in spherical coordinates

Starting from (14)-(15), we have (see Figure 1):

$$u_r := \frac{M(\theta,\phi)}{r(\theta,\phi)} = \begin{pmatrix} \sin\theta\cos\phi \\ \sin\theta\sin\phi \\ \cos\theta \end{pmatrix}, \qquad u_\theta := \frac{\partial_\theta u_r}{\|\partial_\theta u_r\|} = \begin{pmatrix} \cos\theta\cos\phi \\ \cos\theta\sin\phi \\ -\sin\theta \end{pmatrix},$$

and

$$u_\phi := \frac{\partial_\phi u_r}{\|\partial_\phi u_r\|} = \begin{pmatrix} -\sin\phi \\ \cos\phi \\ 0 \end{pmatrix}.$$

The new system $\mathcal{S} = (u_r, u_\theta, u_\phi)$ is mobile and depends on the surface point M. The coordinates of $\overrightarrow{CM}$ in this new system are $(r, 0, 0)^\top_{\mathcal{S}}$.
The two vectors $\partial_\theta M$ and $\partial_\phi M$ form a basis in the plane orthogonal to the normal direction $\widehat{n}(\theta, \phi)$ at the point $M = M(\theta, \phi)$. Since $\overrightarrow{CM} = r u_r$, we have

$$\partial_\theta M = r_\theta u_r + r u_\theta \quad \text{and} \quad \partial_\phi M = r_\phi u_r + r \sin\theta u_\phi,$$

and then

$$\partial_\theta M = (r_\theta, r, 0)^\top_{\mathcal{S}} \quad \text{and} \quad \partial_\phi M = (r_\phi, 0, r\sin\theta)^\top_{\mathcal{S}}.$$

We can write the coordinates of the normal vector in the new system $\mathcal{S}$ as

$$\widehat{n}(\theta, \phi) = \pm \frac{\partial_\theta M \times \partial_\phi M}{\|\partial_\theta M \times \partial_\phi M\|} = \pm \frac{(r\sin\theta, -r_\theta \sin\theta, -r_\phi)^\top_{\mathcal{S}}}{((r^2 + {r_\theta}^2)\sin^2\theta + {r_\phi}^2)^{1/2}}. \tag{56}$$

Knowing that in each visible point M, the normal $\widehat{n}$ points towards C, and knowing that $\sin\theta \geq 0$, it follows that the right sign in (56) is equal to $-$, so we have:

$$\omega(\theta, \phi) \cdot \widehat{n}(\theta, \phi) = (-1, 0, 0)^\top_{\mathcal{S}} \cdot \frac{(-r\sin\theta, r_\theta \sin\theta, r_\phi)^\top_{\mathcal{S}}}{((r^2 + {r_\theta}^2)\sin^2\theta + {r_\phi}^2)^{1/2}}.$$

In conclusion, Equation (13) can be written as

$$\frac{\sin\theta}{r((r^2 + {r_\theta}^2)\sin^2\theta + {r_\phi}^2)^{1/2}} = I$$

or, in an equivalent form, as (17).

References

[1] G. Barles and P. E. Souganidis, *Convergence of approximation schemes for fully nonlinear second order equations*, Asymptotic Analysis, 4 (1991), pp. 271–283.

[2] A. Blake, A. Zisserman, and G. Knowles, *Surface descriptions from stereo and shading*, Imag. and Vis. Comp., 3 (1985), pp. 183–191.

[3] M. Breuss, *The implicit upwind method for 1-D scalar conservation laws with continuous flux*, SIAM J. Numer. Anal., 43 (2005), pp. 970–986.

[4] M. Breuss, E. Cristiani, J.-D. Durou, M. Falcone, and O. Vogel, *Numerical algorithms for Perspective Shape from Shading*, Kybernetika, 46 (2010), pp. 207–225.

[5] M. J. Brooks, W. Chojnacki, and R. Kozera, *Circularly symmetric Eikonal equations and non-uniqueness in computer vision*, J. Math. Anal. Appl., 165 (1992), pp. 192–215.

[6] A. R. Bruss, *The Eikonal equation: some results applicable to computer vision*, J. Math. Phys., 23 (1982), pp. 890–896.

[7] F. Camilli and L. Grüne, *Numerical approximation of the maximal solutions for a class of degenerate Hamilton-Jacobi equations*, SIAM J. Numer. Anal., 38 (2000), pp. 1540–1560.

[8] F. Courteille, A. Crouzil, J.-D Durou, and P. Gurdjos, *Towards shape from shading under realistic photographic conditions*, in Proc. 17$^{\text{th}}$ Int. Conf. Patt. Recog. (vol. II), Cambridge, UK, 2004, pp. 277–280.

[9] F. Courteille, A. Crouzil, J.-D Durou, and P. Gurdjos, *Shape from Shading for the digitization of curved documents*, Mach. Vis. Appl., 18 (2007), pp. 301–316.

[10] E. Cristiani, *Fast Marching and Semi-Lagrangian methods for Hamilton-Jacobi equations with applications*, PhD thesis, Dipartimento di Metodi e Modelli Matematici per le Scienze Applicate, Università di Roma "La Sapienza", Rome, Italy, 2007.

[11] E. Cristiani, M. Falcone, and A. Seghini, *Some remarks on perspective Shape-from-Shading models*, in Proc. 1$^{\text{st}}$ Int. Conf. Scale Space and Variational Methods in Computer Vision, Ischia, Italy, 2007, F. Sgallari, A. Murli, and N. Paragios, eds., vol. 4485 of LNCS, pp. 276–287.

[12] J.-D. Durou, M. Falcone, and M. Sagona, *Numerical methods for Shape-from-Shading: A new survey with benchmarks*, Comp. Vis. and Image Underst., 109 (2008), pp. 22–43.

[13] J.-D. Durou and D. Piau, *Ambiguous Shape from Shading with critical points*, J. Math. Im. Vis., 12 (2000), pp. 99–108.

[14] M. Falcone, M. Sagona, *An algorithm for the global solution of the Shape-from-Shading model*, in Proc. 9$^{\text{th}}$ Int. Conf. Im. Anal. Proc. (vol. I), Florence, Italy, 1997, pp. 596–603.

[15] B.K.P. Horn, *Obtaining shape from shading information*, in: The Psychology of Computer Vision, P.H. Winston, ed., McGraw-Hill, 1975, ch. 4, pp. 115–155.

[16] B.K.P. Horn, *Robot vision*, MIT Press, 1986.

[17] B.K.P. Horn and M.J. Brooks, *Shape from Shading*, Artificial Intelligence Series, MIT Press, 1989.

[18] R. Kimmel, K. Siddiqi, B.B. Kimia, and A. Bruckstein, *Shape from shading: Level set propagation and viscosity solutions*, Int. J. Comput. Vision, 16 (1995), pp. 107–133.

[19] P.-L. Lions, E. Rouy, and A. Tourin, *Shape-from-Shading, viscosity solutions and edges*, Numer. Math., 64 (1993), pp. 323–353.

[20] T. Okatani and K. Deguchi, *Shape reconstruction from an endoscope image by Shape from Shading technique for a point light source at the projection center*, Comp. Vis. and Image Underst., 66 (1997), pp. 119–131.

[21] J. Oliensis, *Uniqueness in Shape from Shading*, Int. J. Comput. Vision, 6 (1991), pp. 75–104.

[22] E. Prados, F. Camilli, and O. Faugeras, *A unifying and rigorous shape from shading method adapted to realistic data and applications*, J. Math. Imag. and Vis., 25 (2006), pp. 307–328.

[23] E. Prados, F. Camilli, and O. Faugeras, *A viscosity solution method for shape-from-shading without image boundary data*, M2AN Math. Model. Numer. Anal., 40 (2006), pp. 393–412.

[24] E. Prados and O. Faugeras, *"Perspective Shape from Shading" and viscosity solutions*, in Proc. 9$^{\text{th}}$ IEEE Int. Conf. Comp. Vis. (vol. II), Nice, France, 2003, pp. 826–831.

[25] E. Prados and O. Faugeras, *Unifying approaches and removing unrealistic assumptions in Shape From Shading: Mathematics can help*, in Proc. 8$^{\text{th}}$ Eur. Conf. Comp. Vis. (vol. IV), Prague, Czech Republic, 2004, vol. 3024 of LNCS, pp. 141–154.

[26] E. Prados and O. Faugeras, *A generic and provably convergent Shape-From-Shading Method for Orthographic and Pinhole Cameras*, Int. J. Comput. Vision, 65 (2005), pp. 97–125.

[27] E. Prados and O. Faugeras, *Shape from Shading: a well-posed problem?*, in Proc. IEEE Conf. Comp. Vis. and Patt. Recog (vol. II), San Diego, California, USA, 2005, pp. 870–877.

[28] E. Prados, O. Faugeras, and F. Camilli, *Shape from Shading: a well-posed problem?*, Rapport de Recherche RR-5297, INRIA Sophia Antipolis, 2004.

[29] E. Rouy and A. Tourin, *A viscosity solutions approach to Shape-from-Shading*, SIAM J. Numer. Anal., 29 (1992), pp. 867–884.

[30] A. Tankus, N. Sochen, and Y. Yeshurun, *A new perspective [on] Shape-from-Shading*, in Proc. 9$^{\text{th}}$ IEEE Int. Conf. Comp. Vis. (vol. II), Nice, France, 2003, pp. 862–869.

[31] A. Tankus, N. Sochen, and Y. Yeshurun, *Perspective Shape-from-Shading by Fast Marching*, in Proc. IEEE Conf. Comp. Vis. and Patt. Recog. (vol. I), Washington, D.C., USA, 2004, pp. 43–49.

[32] O. Vogel, M. Breuss, T. Leichtweis and J. Weickert, *Fast shape from shading for Phong-type surfaces*, in Proc. 2nd Int. Conf. Scale Space and Variational Methods in Computer Vision, Voss, Norway, 2009, X.-C. Tai, K. Mørken, M. Lysaker, K.-A. Lie, eds., vol. 5567 of LNCS, pp. 733–744.

[33] O. Vogel, M. Breuss, and J. Weickert, *A direct numerical approach to perspective Shape-from-Shading*, in Proc. Vision, Modeling, and Visualization Workshop, Saarbrücken, Germany, 2007, H. Lensch, B. Rosenhahn, H.-P. Seidel, P. Slusallek, and J. Weickert, eds., pp. 91–100.

[34] R. Zhang, P.-S. Tsai, J.E. Cryer, and M. Shah, *Shape from Shading: A survey*, IEEE Trans. Patt. Anal. Mach. Intell., 21 (1999), pp. 690–706.